

Journal of Quality Technology

A Quarterly Journal of Methods, Applications and Related Topics

ISSN: 0022-4065 (Print) 2575-6230 (Online) Journal homepage: https://www.tandfonline.com/loi/ujqt20

Degradation under dynamic operating conditions: Modeling, competing processes and applications

Mohammadmahdi Hajiha, Xiao Liu & Yili Hong

To cite this article: Mohammadmahdi Hajiha, Xiao Liu & Yili Hong (2020): Degradation under dynamic operating conditions: Modeling, competing processes and applications, Journal of Quality Technology, DOI: 10.1080/00224065.2020.1757390

To link to this article: https://doi.org/10.1080/00224065.2020.1757390

	Published online: 18 May 2020.
	Submit your article to this journal 🗗
ılıl	Article views: 82
a a	View related articles 🗗
CrossMark	View Crossmark data 🗗





Degradation under dynamic operating conditions: Modeling, competing processes and applications

Mohammadmahdi Hajiha^a, Xiao Liu^a, and Yili Hong^b

^aDepartment of Industrial Engineering, University of Arkansas, Fayetteville, Arkansas; ^bDepartment of Statistics, Virginia Tech, Blacksburg, Virginia

ABSTRACT

This paper investigates degradation modeling under dynamic conditions and its applications. Both univariate and multiple competing degradation processes are considered with individual degradation paths being described by Wiener processes. Parametric and non-parametric approaches are used to capture the effect of environmental conditions on process parameters. For competing degradation processes, we obtain the probability that a particular process reaches a pre-defined threshold, before other processes, over future time intervals. In particular, we consider the potential statistical dependence among the latent remaining lifetimes of multiple degradation processes due to unobserved future environmental factors. Two case studies, aircraft piston pump wear and US highway performance deterioration, are presented. Comprehensive comparison studies are also performed to generate some critical insights on the proposed approach. Data have been made available on GitHub.

KEYWORDS

aircraft piston pump degradation; competing risks; degradation; frailty; highway pavement performance degradation; reliability; Wiener process

1. Introduction

Advances in sensing technologies enable the monitoring of degradation processes under dynamic operating and environmental conditions. System operating and environmental data, also known as the SOE data, represent one of the most significant trends in modern reliability analysis in the age of Big Data (Hong, Zhang, and Meeker 2018; Meeker and Hong 2014). Compared to traditional degradation data, SOE data not only contain critical information on system field variation, but also enable the real-time estimation of system remaining useful life (Bian, Gebraeel, and Kharoufeh 2015; Elsayed 2012; Elwany and Gebraeel 2009; Fang, Paynabar, and Gebraeel 2019; Gebraeel and Pan 2008; Liu et al. 2013; 2020; Tian and Liao 2011; Ye and Chen 2014; Zhao, Xu, and Liu 2018).

1.1. Motivating examples

Two motivating examples are firstly presented and revisited in Section 3.

1.1.1. Motivating example I: Degradation of aircraft hydraulic piston pump

Hydraulic piston pump, shown in Figure 1, is a critical component of an aircraft hydraulic system. The

pistons are designed to complete suction and discharge of fluid alternatively in a reciprocating motion. The hydraulic piston pump is subject to degradation due to a number of reasons. Accumulation of contaminated particles between the valve plate and cylinder block surface causes three-dimensional abrasive wear leading to fluid leakage. The instability of oil film causes abrasive contact between piston bore and piston surface exacerbates the leakage problem. The sliding motion under lubrication causes swash plate and slippers abrasive wear. Because these systems generally have long lifetime, failure data are scarce and degradation data provide important information on the reliability modeling and prediction of aircraft hydraulic piston pump.

The wear rate of aircraft hydraulic piston pump depends on two critical operating conditions: the angular speed ω_b and the discharge pressure p_t . The physical wear mechanism is known and given by the following wear model (Ma et al. 2019):

$$\frac{dx_t}{dt} \propto p_t^{\theta_1} \omega_t^{\theta_2} \exp\left(\theta_3 p_t + \theta_4 \omega_t\right)$$
 [1]

where x_t is the amount of wear, and $\{\theta_i\}_{i=1}^4$ are model parameters which need to be estimated from degradation data. As an illustrative example, Figure 2 shows

the (standardized) degradation, discharge pressure and rotational speed based on a lab testing data set.

1.1.2. Motivating example II: Long-term pavement performance degradation

Highway performance degradation refers to the evolution of crack length on highway sections under dynamic use conditions. The data are available from the Long-Term Pavement Performance (LTPP) program, Federal Highway Administration (LTPP 2019). As an illustration, Figure 3 shows the highway performance index and standardized AADT (Annual Average Daily Traffic) of Highway 16, Yellow Head County, Alberta, Canada. The highway performance deteriorates over time under the influence of AADT. Unlike the first motivating example where the physical degradation mechanism is well understood, the parametric relationship between highway performance and AADT is not available and usually subject to a high degree of uncertainty.

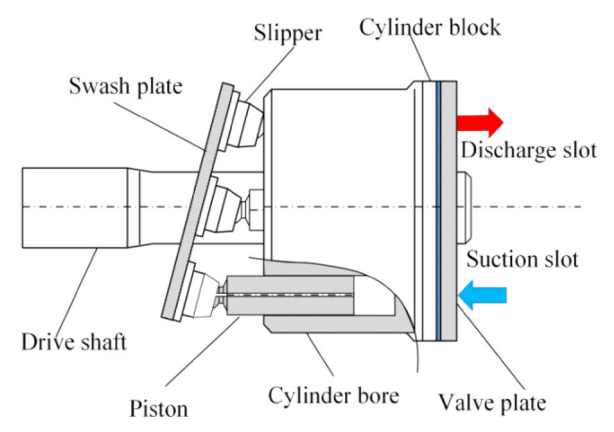


Figure 1. Aircraft hydraulic piston pump with physical wear mechanism.

1.2. Literature review

Degradation models, without explicitly considering the environmental and operating conditions, have been extensively investigated over the last two decades. An important class of degradation models, motivated by the early work of Birnbaum and Saunders (1969), Bhattacharyya and Fries (1982) and Doksum, Hóyland, and Hoyland (1992), focuses on the modeling of degradation using stochastic processes, including Wiener process (Tseng and Peng 2004), Gamma process (Chen and Ye 2018; Jiang, Feng, and Coit 2015; Singpurwalla 1995), Inverse Gaussian process (Chen and Ye 2018; Ye and Chen 2014), and random fields for spatio-temporal degradation data (Liu, Yeo, and Kalagnanam 2018). Stochastic processes allows us not only to model the temporal correlation structure of a degradation process, but also to leverage the well-established mathematical properties, such as sample path properties and transition density.

The modeling of degradation data under changing environments has received much attention in recent years (Bian and Gebraeel 2012; Elwany and Gebraeel 2009; Gebraeel and Pan 2008; Hong et al. 2015; Liao and Tian 2013; Zhai and Ye 2018). Figure 4 summarizes the main modeling strategies for environmental conditions and degradation processes, while Table 1 highlights the main differences of some selected work based on the modeling strategies.

In terms of the modeling of environmental conditions, both stochastic and deterministic models have been adopted as shown in Figure 4. For example, Kharoufeh (2003) and Bian, Gebraeel, and Kharoufeh (2015) modeled environmental condition by continuous-time Markov chain (CTMC), Zhou, Serban, and Gebraeel (2014) modeled environmental conditions by a multinational distribution, while Hong et al. (2015) considered the case where environmental conditions are

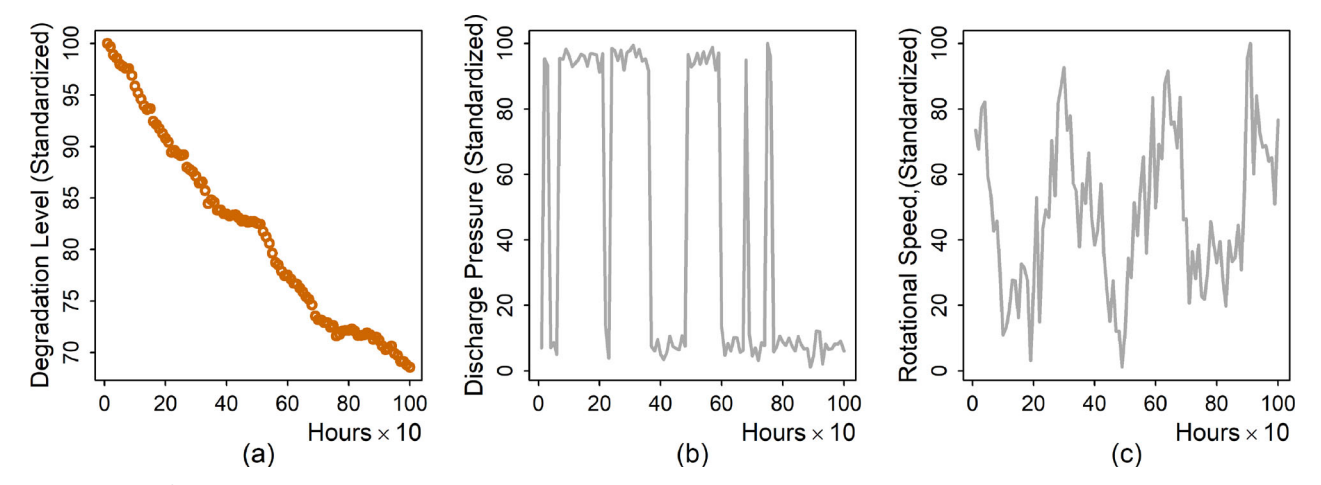


Figure 2. Aircraft hydraulic piston pump degradation: (a) standardized degradation level, (b) standardized discharge pressure, and (c) standardized rotational speed.

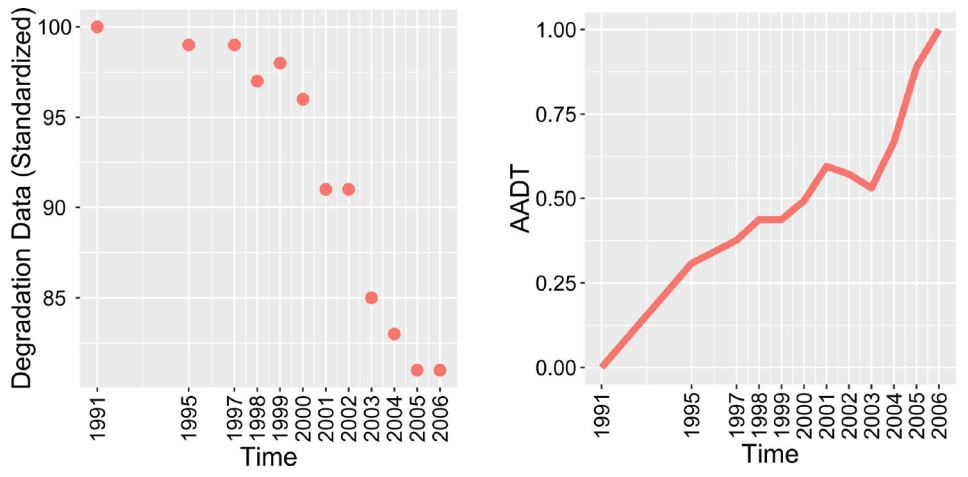


Figure 3. Degradation of Highway 16, Yellow Head County, Alberta, Canada (Left panel: highway performance index; Right panel: standardized annual average daily traffic).

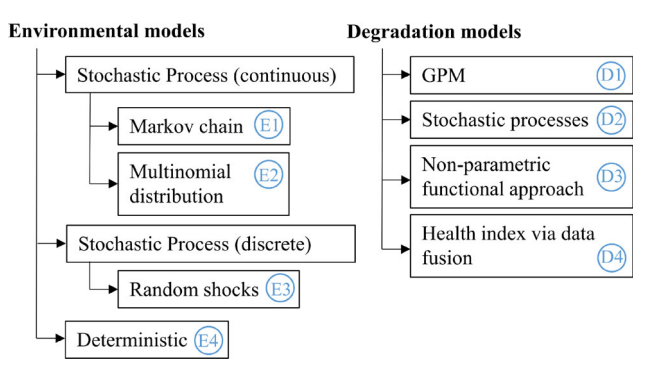


Figure 4. Modeling approaches for environmental conditions and degradation processes.

given by deterministic functions of time. Shen and Cui (2016) considered systems operating in K different environments. Stochastic processes are used to model the transition between environmental regimes as well as the transition of system states within a regime. Random environmental shocks, which cause instantaneous changes to degradation level, have also been considered (Huang et al. 2019; Jiang, Feng, and Coit 2015; Rafiee, Feng, and Coit 2014; Yang et al. 2018). For example, Yang et al. (2018) considered a process whose hazard rate of sudden failure is affected by random shocks induced by environment following non-homogeneous Poisson distribution. Huang et al. (2019) considered an environmental shock as a sharp increase in stress level over a short period of time that causes a sudden increase in degradation level. Jiang, Feng, and Coit (2015) proposed a Gamma degradation model considering i.i.d. shocks arriving according to a homogeneous Poisson process.

In terms of how the degradation process is modeled, important modeling strategies include the general path model (Hong et al. 2015, Hong, Tan, and Ye 2019), stochastic processes (Bian, Gebraeel, and

Table 1. Selected work in degradation modeling under dynamic conditions.

Environmental models	Degradation models	Selected work
E1	D2	Kharoufeh (2003); Bian, Gebraeel, and Kharoufeh (2015); Shen and Cui (2016)
E2	D3	Zhou, Serban, and Gebraeel (2014)
E3	D1	Rafiee, Feng, and Coit (2014)
E3	D2	Jiang, Feng, and Coit (2015)
E4	D1	Hong et al. (2015); Jin et al. (2019); Thomas et al. (2019)
E4	D2	Bian and Gebraeel (2013); Liao and Tian (2013); Huang et al. (2019)
E4	D1, D4	Yan et al. (2016); Liu, Chehade, and Song (2017); Song, Liu, and Zhang (2018)
E4	D2, D3	Hong, Tan, and Ye (2019)

Kharoufeh 2015; Bian and Gebraeel 2013; Kharoufeh 2003; Liao and Tian 2013), and non-parametric functional approach (Zhou, Serban, and Gebraeel 2014). Thomas et al. (2019) modeled the degradation rate of lithium-ion cells as a function of environmental conditions (temperature) and the current degradation. Hong, Tan, and Ye (2019) investigated the oxidation process due to emerging contaminants. The model accounts for the joint effect of agents on degradation rate via shape-restricted Bernstein bases. Zhai and Ye (2018) presented a Wiener process degradation model that considers the correlation of units in the same operating conditions, i.e., the block effect.

The modeling of multivariate degradation processes under dynamic environments is relatively scarce in the literature. One approach relies on a constructed composite Health Index (HI) for degradation modeling and prognostics by fuzing data collected from multiple sensors (Chehade et al. 2018; Liu, Chehade, and Song 2017; Song, Liu, and Zhang 2018; Yan et al. 2016). Such an approach converts the modeling of

multiple sensor signals to a univariate health index, which provides a better characterization of system conditions than individual sensor data. Peng et al. (2016) also investigated the Bayesian degradation analysis of complex systems with multiple degradation indicators under dynamic conditions. One challenge in the modeling of multiple degradation processes arises from the potential dependence among processes. Zhao, Xu, and Liu (2018) investigated the ADT planning with competing failure modes, Liu, Tan, and Pare (2017) proposed a physics-based dynamical model for multiple degradation processes of system internal states under dynamic operating conditions, Liu et al. (2020) considered multiple dependent degradation processes and environmental influence. Fang, Pan, and Hong (2020) investigated the reliability analysis for coherent systems subject to multiple correlated degradation processes. In the above-mentioned literature, Copula has been used to establish the dependence among degradation processes.

1.3. Overview

This paper investigates the modeling of both univariate and multiple competing degradation processes under dynamic conditions. Key contributions of this paper include: i) For multiple degradation processes under the classical setup of competing risks model, we obtain the probability that a particular process reaches a predefined threshold, before other processes, over a given future time interval. In particular, a frailty model is proposed to capture the potential statistical dependence among latent remaining lifetimes of multiple degradation processes due to unobserved future environmental factors; ii) We investigate both parametric and nonparametric approaches to capture the effects of multiple operating and environmental conditions. Such effects are embedded within the classical Wiener degradation process originated from the Nelson's Cumulative Exposure model, i.e., individual degradation processes are modeled by Wiener processes with both the drift and diffusion coefficients being proportionally influenced by common environmental conditions; iii) We perform comprehensive numerical studies, including comparison studies, of the proposed approaches based on real data from two different applications. For the second case study, the processed US highway performance degradation data (LTPP 2019) have been made publicly available for future research and benchmarking.

Section 2 presents the basic modeling framework for degradation data under dynamic conditions. In Section 2.1, we obtain the probability that a system

fails due to a particular degradation process within a given future time interval. Section 2.2 investigates the degradation modeling under changing environmental conditions for individual processes. Two case studies and a numerical example are given in Section 3 to illustrate the model and provide some useful insights on system degradation under changing environmental conditions. Section 4 concludes the paper.

2. Degradation modeling under dynamic conditions

We start with a general scenario where a system is subject to n ($n \ge 1$) degradation processes (n = 1 for the univariate case). Each degradation process i, i = 1, ..., n, is influenced by time-varying conditions, and is modeled by a measurable real-valued stochastic process

$$X_t^{(i)}:[0,\infty) o \mathbb{R}$$
 [2]

where $X_t^{(i)}$ represents the degradation level at time tfor process i. Associated with each process there exists a failure threshold $\eta^{(i)}$. Without loss of generality, we assume that $\eta^{(i)} = 0$ and $x_0^{(i)} > 0$. Based on the classical competing risks model, the system fails when any of the n degradation processes hits its failure threshold, and the system lifetime is given by:

$$T = \min\{T^{(1)}, T^{(2)}, ..., T^{(n)}\}$$
 [3]

where $T^{(i)} = \inf(t : X_t^{(i)} \le 0)$ is the *latent* First-Passage-Time (FPT) for process i. In a special case when n = 1, the system lifetime is simply written as $T = T^{(1)}$.

Equation [3] requires us to (i) investigate the distribution of T (Section 2.1), (ii) obtain the latent FPT for individual degradation processes under dynamic conditions (Section 2.2), and (iii) perform statistical inference given the observed degradation data (Section 2.2.3).

2.1. The overall framework

From reliability prediction and system prognostics point of view, of central interest is the distribution of T in Eq. [3]. In particular, we are concerned with an important question frequently arising from engineering practice: at time \tilde{t} , what is the probability $P_{\Lambda}^{(i)}$ that the system fails due to process i within a future time interval $(\tilde{t}, \tilde{t} + \Delta]$, provided with the last available degradation measurement taken at time $\tau < \tilde{t}$? In other words, we are interested in the probability that a particular degradation process hits its threshold before other processes over $(\tilde{t}, \tilde{t} + \Delta]$. This scenario is illustrated in Figure 5.

Note that, the probability $P_{\Delta}^{(i)}$ depends on whether the multiple degradation processes are stochastically dependent for $t > \tau$. For any process i, let $x_{\tau}^{(i)}$ be the last available degradation measurement at time τ , and let $F^{(i)}(\nu^{(i)}; x_{\tau}^{(i)})$ be the distribution of the latent remaining lifetime $\nu^{(i)}$ for process i given the degradation level $x_{\tau}^{(i)}$ at time τ . Then, Propositions 1 and 2 respectively show how the probability $P_{\Delta}^{(i)}$ can be found for independent and dependent cases.

Proposition 1: System Reliability (Independent Case). If all degradation processes are stochastically independent for all $t > \tau$, and the system functions at time \tilde{t} $(>\tau)$, then, the probability that the system fails due to degradation process i, i = 1, ..., n, within the interval $(\tilde{t}, \tilde{t} + \Delta)$ is

$$P_{\Delta}^{(i)} = \int_{0}^{\Delta} \left\{ \xi_{1}(\nu^{(1)}, ..., \nu^{(i-1)}, \nu^{(i+1)}, ..., \nu^{(n)}) \xi_{2}(\nu^{(i)}) \right\}_{\nu.1_{n}} d\nu$$
[4]

where

$$\xi_{1}(\nu^{(1)},...,\nu^{(i-1)},\nu^{(i+1)},...,\nu^{(n)})$$

$$=\prod_{i=1,j\neq i}^{n}\int_{0}^{\infty}(1-F^{(i)}(\nu^{(j)};u))p^{(i)}(u,\tilde{t};x_{\tau}^{(j)})du \qquad [5]$$

$$\xi_2(\nu^{(i)}) = \frac{\partial}{\partial \nu^{(i)}} \int_0^\infty F^{(i)}(\nu^{(i)}; u) p^{(i)}(u, \tilde{t}; x_{\tau}^{(i)}) du.$$
 [6]

and $p^{(i)}(u, \tilde{t}; x_{\tau}^{(i)})$ is the transition density for process i from degradation level x_{τ} at time τ to degradation level *u* at time $\tilde{t} > \tau$.

This proposition can be shown as follows. For independent degradation processes, the joint system survival function is:

$$G(\nu^{(1)}, \nu^{(2)}, ..., \nu^{(n)}) = \prod_{i=1}^{n} (1 - F^{(i)}(\nu^{(i)}; \mathbf{x}_{\tilde{t}}^{(i)}))$$
 [7]

where $x\tilde{t}^{(i)}$ is the (unobserved) degradation level at time $\tilde{t}(>\tau)$, and

$$F^{(i)}(\nu^{(i)}; x_{\tilde{t}}^{(i)}) = \int_0^\infty F^{(i)}(\nu^{(i)}; u) p^{(i)}(u, \tilde{t}; x_{\tau}^{(i)}) du.$$
 [8]

Hence, it follows from Crowder (2001) that the sub-density of the latent remaining lifetime for any process i is given by

$$\begin{split} f_{sub}^{(i)}(\nu) &= \left\{ -\frac{\partial G(\nu^{(1)}, \nu^{(2)}, ..., \nu^{(n)})}{\partial \nu^{(i)}} \right\} \\ &= \left\{ \xi_1(\nu^{(1)}, ..., \nu^{(i-1)}, \nu^{(i+1)}, ..., \nu^{(n)}) \xi_2(\nu^{(i)}) \right\}_{\nu \cdot 1_n} \end{split}$$

where $\xi_1(\cdot)$ and $\xi_2(\cdot)$ are given by Eqs. [5] and [6]. Finally, the probability that the system fails due to

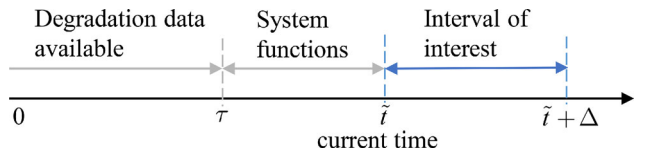


Figure 5. The scenario considered in this paper: τ is the time when the last degradation measurement is taken; $(\tau, \tilde{t}]$ is the interval over which the system properly functions; and $(\tilde{t}, \tilde{t} +$ Δ is the interval over which the system reliability is of interest.

degradation process i within the interval $(\tilde{t}, \tilde{t} + \Delta)$ is obtained from the sub-density as follows:

$$\begin{array}{ll} P_{\Delta}^{(i)} &= \int_{0}^{\Delta} f_{sub}^{(i)}(\nu) d\nu \\ &= \int_{0}^{\Delta} \left\{ \xi_{1}(\nu^{(1)},...,\nu^{(i-1)},\nu^{(i+1)},...,\nu^{(n)}) \xi_{2}(\nu^{(i)}) \right\}_{\nu \cdot 1_{n}} d\nu. \end{array}$$

The proposition above assumes that the multiple degradation processes are stochastically independent for all $t > \tau$, which is not always the case in reality. As shown in Figure 5, although the historical environmental condition can be observed up to \tilde{t} , the future environmental condition beyond \tilde{t} is rarely known exactly. It is possible that the future degradation processes are influenced by some common but unobserved random factor Z^* . As a result, the latent remaining lifetimes, $\nu^{(1)}, \nu^{(2)}, ..., \nu^{(n)}$, corresponding to the *n* processes become stochastically dependent. Hence, it is natural to assume that the latent remaining lifetimes would become independent if the random factor Z^* was exactly known. This implies that the latent remaining lifetimes are conditionally independent given $Z^* = z^*$:

$$G(\nu^{(1)}, \nu^{(2)}, ..., \nu^{(n)}|z^*) = \exp(-z^*\psi)$$
 and ψ

$$= \sum_{i=1}^n \Lambda^{(i)}(\nu^{(i)})$$
 [11]

where $\Lambda^{(i)}(\nu^{(i)})$ is the cumulative hazard function corresponding to degradation process i and is given by:

$$\Lambda^{(i)}(\nu^{(i)}) = -\log(1 - F^{(i)}(\nu^{(i)}; x_t^{(i)})).$$
 [12]

The random factor Z^* is known as frailty. We adopt a Gamma frailty model by assuming that Z^* follows a Gamma distribution for its flexibility in taking variety of shapes (Abbring and Van Den Berg 2007). Since it is well-known that the Gamma shape and inverse scale parameters are not identifiable in a Gamma frailty model, we assume that Z^* has mean one and variance ω_{Z^*} , and the unconditional system joint survival function becomes (Liu 2012):

$$G(\nu^{(1)}, \nu^{(2)}, ..., \nu^{(n)}) = (1 + \omega_{Z^*} \psi)^{-\frac{1}{\omega_{Z^*}}}.$$
 [13]

Proposition 2: System Reliability (Dependent Case). If the stochastic dependence among competing degradation processes is captured by the frailty model [13] for $t > \tau$, and the system still functions at time $\tilde{t} > \tau$, then, the probability that the system fails due to degradation process i, $i \in [1, ..., n]$, within the interval $(\tilde{t}, \tilde{t} + \Delta]$ is

$$\begin{split} P_{\Delta}^{(i)} &= \int_{0}^{\Delta} \left\{ -\frac{\partial G(\nu^{(1)}, \nu^{(2)}, ..., \nu^{(n)})}{\partial \nu^{(i)}} \right\}_{\nu \cdot 1_{n}} d\nu \\ &= \int_{0}^{\Delta} {\Lambda'}^{(i)}(\nu) \left\{ 1 + \omega_{z^{*}} \sum_{j=1, i \neq j}^{n} {\Lambda}^{(j)}(\nu) \right\}^{-\frac{1}{\omega_{z^{*}}} - 1} d\nu. \end{split}$$

2.2. Degradation modeling under dynamic conditions

The two propositions above hinge on the distribution $F^{(i)}(\nu^{(i)}; x_{\tau}^{(i)})$ of the latent remaining lifetime $\nu^{(i)}$ given the last available degradation level $x_{\tau}^{(i)}$ at time τ , as well as the transition density $p^{(i)}(u,t;x_{\tau}^{(i)})$. Apparently, both $F^{(i)}(\cdot)$ and $p^{(i)}(\cdot)$ depend on how the degradation process $X_t^{(i)}$ is modeled, which is to be discussed in this subsection. Throughout this section, the superscript $\cdot^{(i)}$ is dropped for simplicity.

Consider a Wiener degradation process, $\{X_t\}_{t\geq 0}$, as follows:

$$X_{t} = x_{0} + \int_{0}^{t} \mu_{s} ds + \int_{0}^{t} \sigma_{s} dB_{s}$$
 [15]

where μ_t and σ_t are the time-dependent drift and diffusion, and $\{B_t\}_{t\geq 0}$ is a standard Wiener process such that: (i) $B_0=0$; (ii) for every $0\leq t_0< t_1< ...< t_m$, the increments $B_{t_1}-B_{t_0}, B_{t_2}-B_{t_1}, ..., B_{t_m}-B_{t_{m-1}}$ are independent random variables; (iii) for each $0\leq s< t<\infty$, the increment B_t-B_s is a Gaussian random variable with mean 0 and variance t-s; and (iv) the sample paths are continuous functions. In a special case when both $\mu_t=\mu_0$ and $\sigma_t=\sigma_0$ for all t, model [15] degenerates to a linear degradation process with time-invariant diffusion, $X_t=x_0+\mu_0 t+\sigma_0 B_t$.

Both μ_t and σ_t are influenced by dynamic conditions, which are described by a q-dimension time series, $z_t = (z_{1,t}, z_{2,t}, ..., z_{q,t})$. To capture the influence of z_t on $\{X_t\}_{t>0}$, we assume the following parameterization:

$$\mu_t = \mu_0 \exp\left\{\sum_{j=1}^q g_j(z_{j,t})\right\} \equiv \mu_0 \kappa_t$$
 [16]

$$\sigma_t^2 = \sigma_0^2 \exp\left\{\sum_{j=1}^q g_j(z_{j,t})\right\} \equiv \sigma_0^2 \kappa_t$$
 [17]

where $g_j(\cdot)$, j = 1, 2, ..., q, captures the effect of the *j*th environmental condition and satisfies:

- $g_j(z)$ is non-decreasing in z, i.e., a harsher environmental condition does not reduce the degradation rate.
- $g_j(z_0) = 0$ which implies that μ_0 and σ_0 are the initial values of μ and σ under the initial environmental condition z_0 .
- κ_t is measurable, i.e., for $t \ge 0$, we have $\int_0^t \kappa_s ds < \infty$.

Equations [16] and [17] indicate that the degradation rate at time t depends only on the environmental conditions at t, regardless of the history of the degradation process. This consideration can be justified by the well-known Nelson's Cumulative Exposure (CE) model (Nelson 2009) originated from the Palmgren-Miner linear damage hypothesis and has been widely adopted in reliability modeling under time-varying conditions (Liao and Elsayed 2006; Liu and Qiu 2011). For degradation process (Eq. [15]), the Nelson's CE model necessarily implies that $X_t = X_{\zeta_t}$ for some time transformation function ζ_t (Doksum, Hóyland, and Hoyland 1992; Peng and Tseng 2010; Ye and Chen 2014). If the first order derivative of ζ_t exists, it follows from Eqs. [15]–[17] that:

$$\int_0^t \mu_s ds = \int_0^{\zeta_t} \mu_0 ds = \mu_0 \zeta_t$$
 [18]

$$\int_{0}^{t} \sigma_{s} dB_{s} = \int_{0}^{\zeta_{t}} \sigma_{0} dB_{s} = \sigma_{0} B_{\zeta_{t}}.$$
 [19]

It is easy to see that the parameterization (Eq. [16]) can be obtained from Eq. [18] by letting $\zeta_t' = \kappa_t$. Since κ_t is measurable, the stochastic integral $\int_0^t \kappa_t^{1/2}(y) dB_y$ exists and has the same distribution as the time-transformed Brownian motion B_{ζ_t} in Eq. [19]. Then, we obtain Eq. [17] from Eq. [19]. Note that, it is implied by Eqs. [16] and [17] that the environmental condition affects both the drift and diffusion such that the ratio between μ_t and σ_t^2 remains unchanged:

$$\frac{\int_0^t \mu_s ds}{\int_0^t \sigma_c^2 ds} = \frac{\mu_t}{\sigma_t^2} = \frac{\mu_0}{\sigma_0^2} = \gamma$$
 [20]

for some constant γ .

Finally, substituting Eqs. [16] and [17] into Eq. [15], we obtain the following degradation process with time-dependent mean-value function and time-dependent diffusion, $X_t = x_0 + m_t + \varepsilon_t$, where $m_t = \mu_0 \int_0^t \kappa_s ds = \mu_0 \zeta_t$ and $\varepsilon_t = \sigma_0 \int_0^t \kappa_s^{1/2} dB_s$. For



measurable κ , the stochastic integral ε_t is Gaussian with mean zero and variance $\sigma_0^2 \zeta_t = \sigma_0^2 \int_0^t \kappa_s ds$.

2.2.1. The effect of environmental conditions, q(z)

The function $g_i(\cdot)$, j = 1, 2, ..., q, captures the effect of the *i*th environmental condition. In this subsection, both parametric and non-parametric approaches are used to model $g_i(z)$. The subscript \cdot_i is omitted in this subsection without ambiguity.

The parametric approach assumes a functional form for g(z) motivated by known physics or engineering domain knowledge. For example, in our first motivating example in Section 1.1, the physical wear mechanism of hydraulic piston pump, under given pressure and rotational speed, is known and can be described by Eq. [1].

When physics or engineering knowledge is not available or too complicated to be utilized, non-parametric models of g(z) become more useful. For example, in our second motivating example in Section 1.1, the degradation of highway concrete asphalt has extremely complex interactions with external environmental factors and is subject to a high degree of uncertainty which cannot be well explained by the first-principle physics model.

Adopting the non-parametric approach, we model g(z) by a linear combination of spline bases (piecewise polynomials). Since $g(z_0) = 0$ and g(z) needs to be non-decreasing in z, shape-restricted splines are required (Hong et al. 2015; Meyer 2008; Ramsay 1998). In particular,

$$g(z) = \sum_{q=1}^{q=b+h} c_q I_q^{(h)}(z), \quad c_q \ge 0$$
 [21]

where h is the order of the spline function, b is the number of knots, $\{c_q\}_{q=1}^{b+h}$ are the coefficients to be estimated, and $I_q^{(h)}(z)$ is the qth I-spline base:

$$I_q^{(h)}(z) = \int_z^z M_q^{(h)}(u) du$$
 [22]

where $M_q^{(h)}(u)$ is the qth base of order h in M-splines which can be computed recursively as

 $z_{\min} = d_1 = \dots = d_h < d_{h+1} < \dots < d_{h+b} < \dots$ $d_{h+1+b} = \dots = d_{2h+b} = z_{\text{max}}$. Since M-splines are nonnegative, Eq. [22] gives non-decreasing bases of Isplines. Hence, g(z) in Eq. [22] is non-decreasing in z for non-negative coefficients of basis functions c_a .

To illustrate the non-parametric approach, we model a simulated degradation data set (shown in 7) using the non-parametric approach described above. Then, the estimated degradation path is compared to that obtained from the parametric approach which assumes the correct relationship between degradation and environmental conditions (i.e., the best-case scenario for the parametric approach). Here, the underlying function $g(\cdot)$ is taken to be $g(z) = \theta^{-1}(z - z_0)$. Figure 6 shows the estimated κ , as a function of the environmental condition z, for different combinations of the order, h, and the number of knots, b. We see that the shape-restricted splines ensure that κ is non-decreasing in z, i.e., the harsher environment condition does not reduce the degradation rate. Table 2 shows the candidate values for the order and knots with the corresponding AIC, BIC, and the maximized log-likelihood (to be discussed in Section 2.2.3). See that, when h=1 and b = 3, the minimum AIC and BIC, and the maximum log-likelihood are achieved.

Table 3 provides the estimated parameters as well as the asymptotic 90 percent confidence intervals for μ , σ and the four coefficients $\{c_i\}_{i=1}^4$ when dataset 1 is used. Figure 7a shows the comparison between the estimated mean degradation paths, respectively obtained from the non-parametric method and the parametric method. In particular, we re-simulate another dataset, and compare the estimated mean degradation paths respectively obtained from the non-parametric method (h=2 and b=4) and the parametric method; see Figure 7b. In both cases, it is worth noting that the non-parametric approach has a performance with comparable the parametric approach which assumes the correct parametric form of $g(\cdot)$ (i.e., the best-case scenario which is in fact unrealistic in practice). The non-parametric approach effectively models the degradation under dynamic

$$M_q^{(h)}(z) = \begin{cases} 1(d_q \le z < d_{q+1}) \frac{1}{d_{q+1} - d_q} & \text{if} \quad h = 1 \\ \frac{h(z - d_q) M_q^{(h-1)}(z) + (d_{q+h} - z) M_{q+1}^{(h-1)}(z)}{(h-1)(d_{q+h} - d_q)} 1(d_q \le z < d_{q+1}) & \text{if} \quad h > 1. \end{cases}$$
 [23]



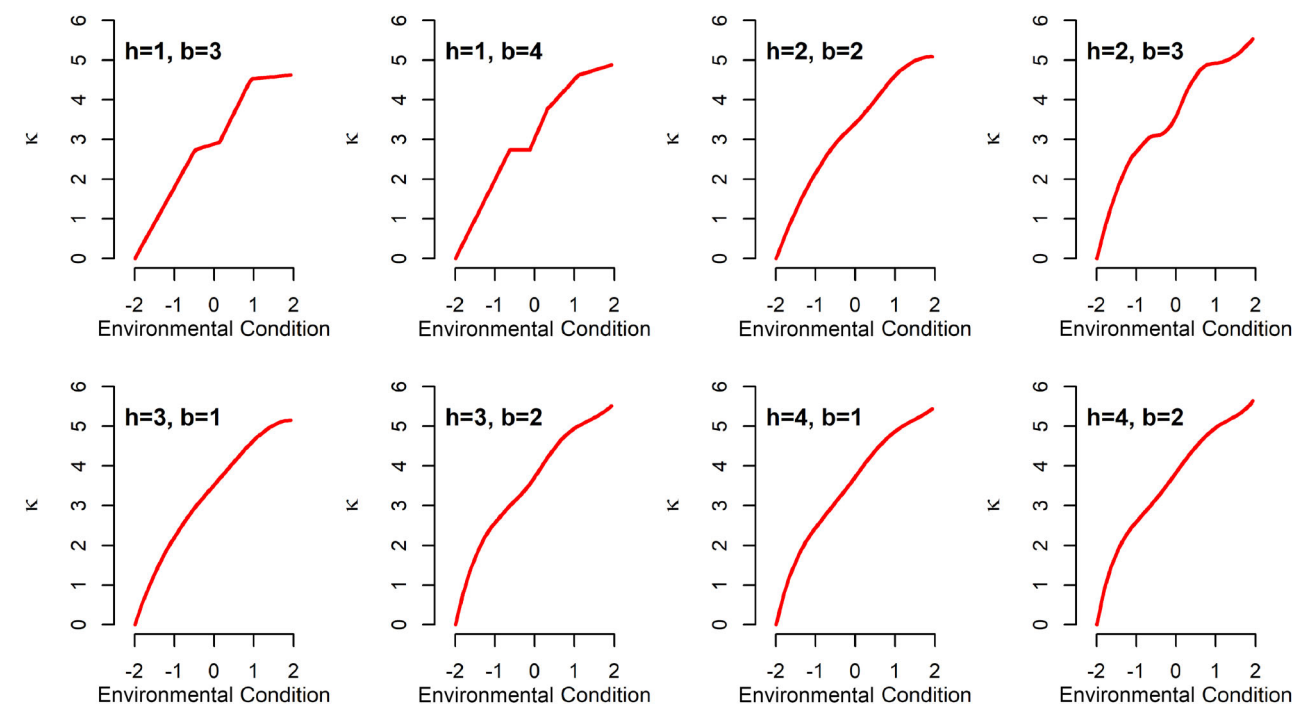


Figure 6. Estimated κ , as a function of the environmental condition z, for different combinations of h and b.

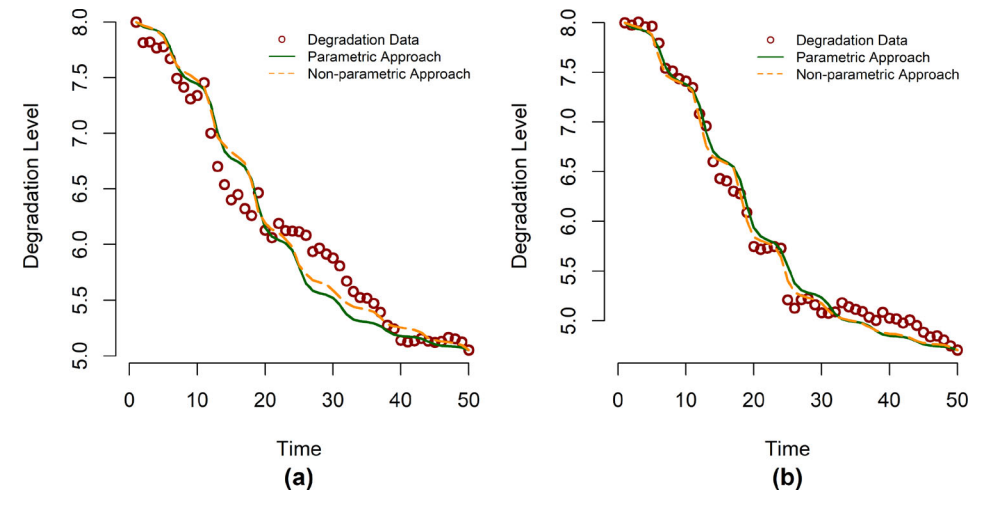


Figure 7. (a) Comparison of non-parametric (h=1 and b=3) and parametric modeling approaches; (b) Comparison of non-parametric metric (h = 2 and b = 4) and parametric modeling approaches based on another simulated dataset.

conditions without making parametric assumptions on $g(\cdot)$.

2.2.2. Latent remaining life

Let $P(u, t; x_{\tau})$ be the probability that a degradation process has not reached a certain level u at time tconditioning on $X_{\tau} = x_{\tau}$. Then, the conditional transition density of the degradation process (Eq. [15]) is

$$p(u,t';x_{\tau}) = \frac{d}{du}P(u,t';x_{\tau})$$
 [24]

where $t' = t - \tau$ is the remaining life. The transition density can be obtained as follows

$$p(u, t'; x_{\tau}) = \frac{1}{2} (\pi s_{t'}^2)^{-1/2} \{ A(u) - \exp(-2x_{\tau}\gamma) B(u) \}$$
[25]

where

$$A(u) = \exp\left\{-\frac{(u - x_{\tau} - m_{t'})^{2}}{4s_{t'}^{2}}\right\},$$

$$B(u) = \exp\left\{-\frac{(u + x_{\tau} - m_{t'})^{2}}{4s_{t'}^{2}}\right\}$$
[26]

and

Table 2. Model selection for different combinations of h and b.

h	b	AIC	BIC	Log-Likelihood	# of Parameters
1	4	-106.897	-92.70559	60.04487	7
1	3	-109.201	-97.548	60.51007	6
2	2	-107.0636	-95.5919	59.53182	6
2	3	-107.2299	-93.8457	60.61493	7
3	1	-106.835	-95.36289	59.41751	6
3	2	-106.1661	-92.7819	60.08303	7
4	1	-105.5677	-92.18355	59.78385	7
4	2	-103.748	-88.45179	59.87399	8

Table 3. Parameter estimation with 90 percent asymptotic confidence intervals for Dataset 1.

Parameters	MLE	Asymptotic 90 percent confidence interval
μ	-0.004	(-0.011, 0.003)
σ	0.025	(0.003, 0.046)
C ₁	1.075	(-1.044, 3.194)
c ₂	1.37	(0.248, 2.491)
<i>c</i> ₃	0.838	(-0.147,1.823)
c ₄	0.633	(-0.311, 1.577)

$$m_{t'} = \mu_0 \int_0^{t'} \kappa_{\tau+s} ds, \quad s_{t'}^2 = \frac{1}{2} \sigma_0^2 \int_0^{t'} \kappa_{\tau+s} ds.$$
 [27]

Hence, conditioning on the degradation level x_{τ} at time τ , the distribution of remaining life for a constant failure threshold $\eta = 0$ can be found as (Cox and Miller 1965):

unimodal under dynamic environmental condition. As shown in Figure 8d, between times 0 and 40, the density function oscillates with the environmental condition. As a result, the probability of failure is notably higher over the time periods when the environmental condition becomes harsher (i.e., the spikes in the density function).

If the degradation process is under discrete environmental conditions (such as the CTMC model considered in Kharoufeh (2003) and Bian, Gebraeel, and Kharoufeh (2015)), we consider a condition specified by a piece-wise constant function, i.e., there exists a partition $0 \le t_1 < t_2 < t_3 < \tau$ such that z_t is a constant on the sub-interval $[t_i, t_{i+1})$ for j = 1, 2. Figure 9 shows the environmental condition, degradation rate, CDF and pdf of the FPT of the degradation process. The effect of the changing environmental condition on the degradation process is clearly shown. For example, when the environmental condition suddenly jumps at time 10, a jump is also observed in the pdf of FPT, leading to a high failure probability between times 10 and 15.

2.2.3. Parameter estimation

Propositions 1 and 2 in Section 2.1 show how the failure probability and failure mode (i.e., $P_{\Lambda}^{(i)}$) can be

$$F(t'; x_{\tau}) = 1 - \int_{0}^{\infty} p(\nu, t'; x_{\tau}) d\nu$$

$$= 1 - \frac{1}{2} \left\{ \left(1 - \operatorname{erf} \left(-\frac{x_{\tau} + m_{t'}}{2s_{t'}} \right) \right) - \exp\left(-2x_{\tau}\gamma \right) \left(1 - \operatorname{erf} \left(-\frac{x_{\tau} + m_{t'}}{2s_{t'}} \right) \right) \right\}$$
[28]

where the error function $erf(\cdot)$ is defined as erf(u) = $2\pi^{-1/2} \int_0^u e^{-t^2} dt$. To obtain the second line on the right-hand-side of Eq. [28], note that

$$\int_{0}^{\infty} A(x)dx = (\pi s_{t'}^{2})^{1/2} \left\{ 1 - \operatorname{erf}\left(-\frac{x_{\tau} + m_{t'}}{2s_{t'}}\right) \right\}$$
 [29]
$$\int_{0}^{\infty} B(x)dx = (\pi s_{t'}^{2})^{1/2} \left\{ 1 - \operatorname{erf}\left(-\frac{x_{\tau} - m_{t'}}{2s_{t'}}\right) \right\}.$$
 [30]

For illustrative purposes, consider a degradation process (Eq. [15]) under dynamic environmental condition with $\mu_0 = -0.5$, $\sigma_0 = 1$, $x_0 = 10$ and $\kappa_t =$ $\exp(\theta^{-1}(z_t-z_0))$. Let the environmental condition be specified by a continuous function $z_t = \sin(0.1t) + \cos(t)$. Figure 8 shows the environmental condition, time-varying degradation rate, CDF and pdf of the FPT of the degradation process. It is worth noting that the pdf of the FPT is no longer

evaluated over any time interval $(\tilde{t}, \tilde{t} + \Delta)$, given that the last available degradation measurement is taken at some time $\tau < t$. Section 2.2 presents the degradation model, FPT distribution, as well as the transition density which are required to evaluate $P_{\Lambda}^{(i)}$. In this section, we focus on estimating the unknown parameters in the degradation model. It is assumed that,

- For degradation process i, i = 1, ..., n, a number of $m^{(i)} + 1$ measurements are taken at discrete times $t^{(i)} = (t_0^{(i)}, t_1^{(i)}, \dots, t_{m^{(i)}}^{(i)})$ over a time period $[0, \tau]$. Here, $0 = t_0^{(i)} < t_1^{(i)} < \dots < t_{m^{(i)}}^{(i)} \le \tau$.
- The observed degradation data are denoted by $\mathbf{x}^{(i)} = (x_0^{(i)}, x_1^{(i)}, \dots, x_{m^{(i)}}^{(i)})$ where $x_0^{(i)}$ is the initial degradation measurement at time 0.
- If the system fails at \tilde{t} due to process i, $c^{(j)} =$ $\tau - t_{m^{(j)}}^{(j)}$ is the censored observation for process j

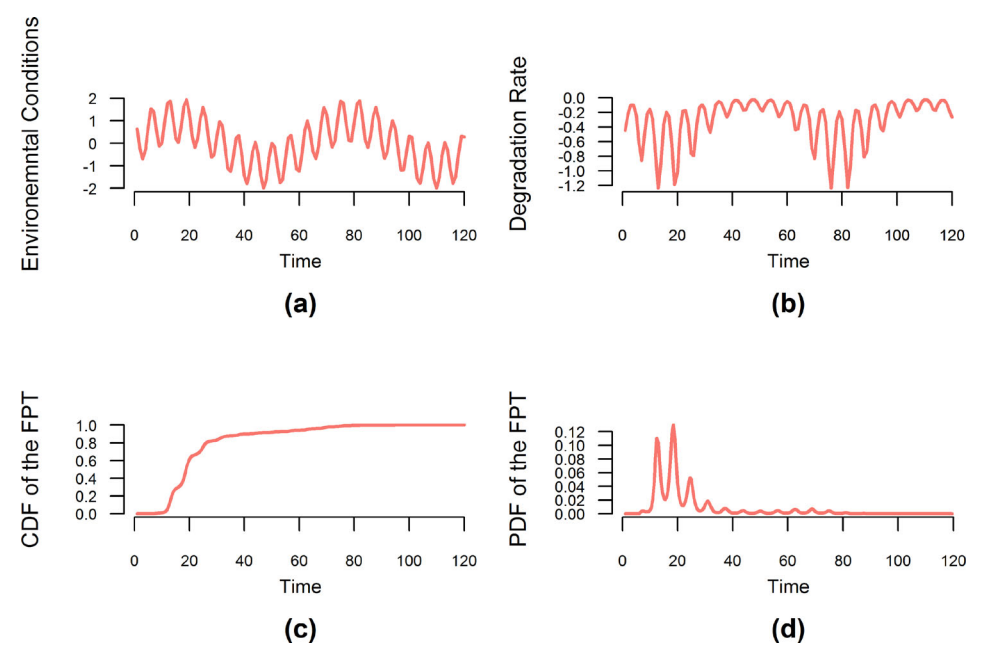


Figure 8. Degradation under continuous dynamic environmental conditions: (a) environmental condition, (b) degradation rate, (c) CDF of the FPT, and (d) pdf of the FPT.

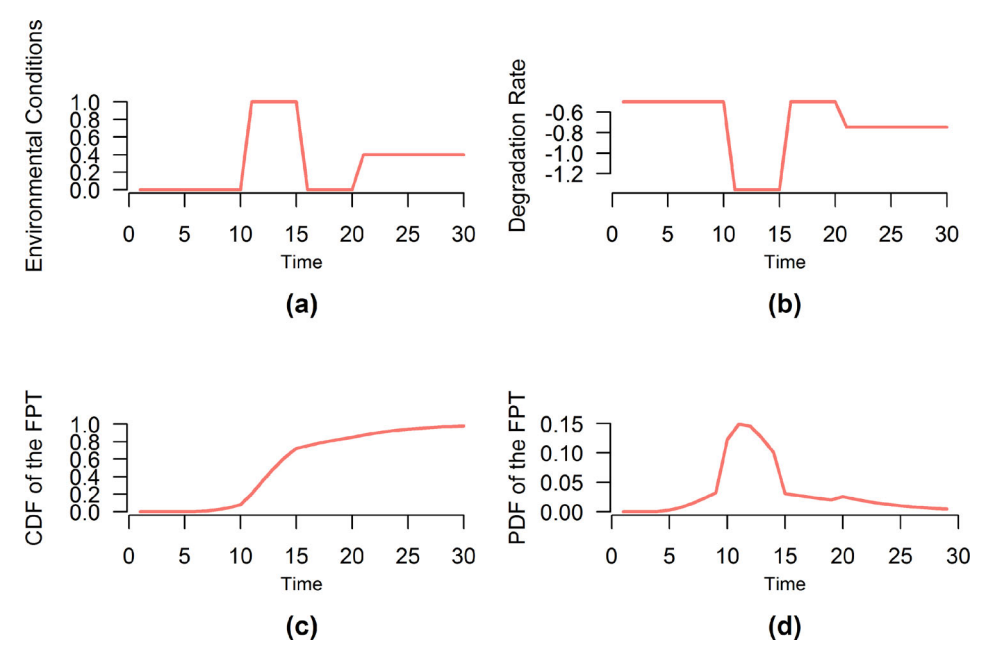


Figure 9. Degradation under discrete environmental conditions: (a) environmental condition, (b) degradation rate, (c) CDF of the FPT, and (d) Multimodal pdf of the FPT.

for $j=1,2,\ldots,n$ and $j\neq i$. If the system still functions at τ , $c^{(i)}=\tau-t_{m^{(i)}}^{(i)}$ is the censored observation for process $i, i=1,2,\ldots,n$.

• The cause of system failure is denoted by the vector $\boldsymbol{\delta} = (\delta^{(1)}, \delta^{(2)}, \dots, \delta^{(n)})$ such that $\delta^{(i)} = 1$ if the failure is due to degradation process i; otherwise $\delta^{(i)} = 0$. Note that under the assumption of competing risks, $\sum_{i=1}^n \delta^{(i)} \leq 1$. if no failure has occurred up to τ , $\sum_{i=1}^n \delta^{(i)} = 0$, i.e. δ is a zero vector.

Then, the likelihood function of the model parameters is

$$\mathbb{L} = \prod_{i=1}^{n} \prod_{j=1}^{m^{(i)}} p(x_{j}^{(i)}, t_{j}^{(i)}; x_{j-1}^{(i)})
\cdot \prod_{i=1}^{n} \prod_{j=1}^{m^{(i)}} p(0, t_{j}^{(i)}; x_{j-1}^{(i)})^{\delta^{(i)}} \cdot \prod_{i=1}^{n} (1 - F(c^{(i)}; x_{m^{(i)}}^{(i)}))^{1 - \delta^{(i)}}$$
[31]

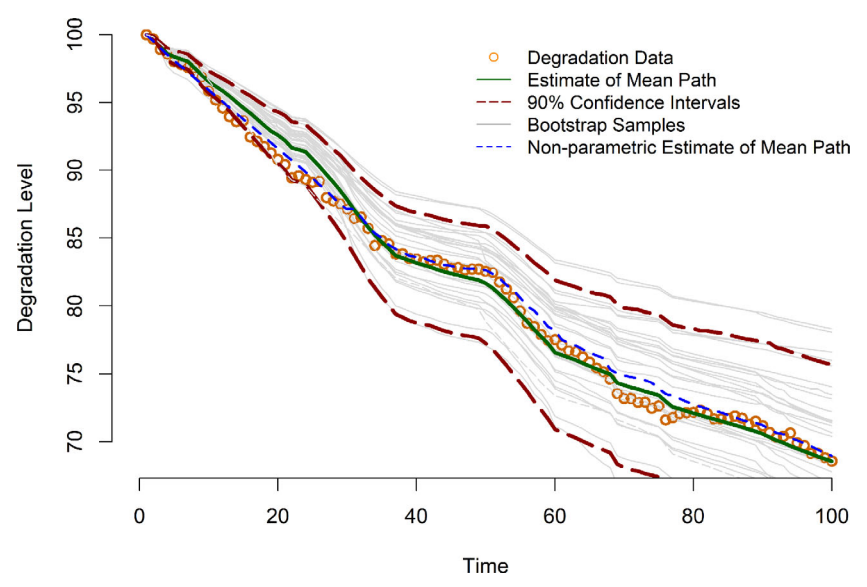


Figure 10. The estimated mean degradation path and the 90 percent bootstrap confidence interval.

The first term on the right-hand-side of Eq. [31] is the contribution to the total likelihood from the observed degradation data, i.e., it is the multiplication of the transition densities of the degradation at time $t_i^{(i)}$, given the observed degradation $x_{i-1}^{(i)}$ at time $t_{i-1}^{(i)}$. The transition density between two consecutive times is given as follows

$$p(x_{j}^{(i)}, t_{j}^{(i)}; x_{j-1}^{(i)}) = \frac{1}{2\sqrt{(\pi S(t_{j-1}^{(i)}, t_{j-1}^{(i)})}} \{A(x_{j-1}^{(i)}) - \exp(-2\gamma x_{j-1}^{(i)}) B(x_{j}^{(i)})\}$$
[32]

where

$$A(x_j^{(i)}) = \exp\left(-\frac{(x_j^{(i)} - x_{j-1}^{(i)} - M(t_{j-1}^{(i)}, t_j^{(i)}))^2}{4S(t_{j-1}^{(i)}, t_j^{(i)})}\right)$$
[33]

$$B(x_j^{(i)}) = \exp\left(-\frac{(x_j^{(i)} + x_{j-1}^{(i)} - M(t_{j-1}^{(i)}, t_j^{(i)}))^2}{4S(t_{j-1}^{(i)}, t_j^{(i)})}\right)$$
[34]

$$M(t_{j-1}^{(i)}, t_j^{(i)}) = \mu_0 \int_{t_{j-1}^{(i)}}^{t_j^{(i)}} \kappa_s ds$$
 [35]

$$S(t_{j-1}^{(i)}, t_j^{(i)}) = \frac{1}{2} \int_{t_{i-1}^{(i)}}^{t_j^{(i)}} \sigma_s^2 ds = \frac{1}{2} \sigma_0^2 (k_j^{(i)} - k_{j-1}^{(i)})$$
 [36]

The second and the third terms on the right-handside of Eq. [31] are the contributions to the total likelihood, respectively, from the observed system lifetime and censored observations. The second term vanishes when no system failure is observed at time τ . Details

Table 4. Parameter estimation for hydraulic piston pump degradation.

Parameters	MLE	Approximate 90 percent confidence interval
μ_0	-0.199	(-0.254, -0.144)
σ_0	0.253	(0.216, 0.290)
$egin{array}{c} \sigma_0 \ heta_1 \end{array}$	-0.119	(-0.707, 0.470)
	0.158	(-0.352, 0.668)
$ \theta_2 \\ \theta_3 \\ \theta_4 $	0.016	(-0.002, 0.034)
θ_4	0.004	(-0.010, 0.018)

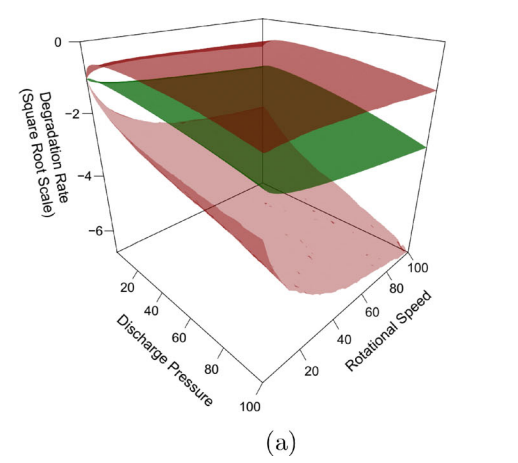
of implementing the MLE as well as obtaining the confidence intervals are provided in the next section.

3. Case studies, numerical examples and comparison

We revisit the two motivating examples in Section 1.1 and illustrate the applications of the proposed approach. The first case study investigates the degradation of aircraft hydraulic piston pump, while the second case study models the highway performance degradation data from the U.S. Federal Highway Administration.

3.1. Case study I: Degradation of aircraft hydraulic piston pump

Aircraft hydraulic piston pump, shown in Figure 1, is a critical component of aircraft hydraulic system. As described in Section 1.1, a hydraulic piston pump does a complete cycle of suction and discharge of fluid in spinning motion. This mechanism is controlled by an engine that rotates the cylinder block and the tilted swash plate connected to the piston bores. Due to the



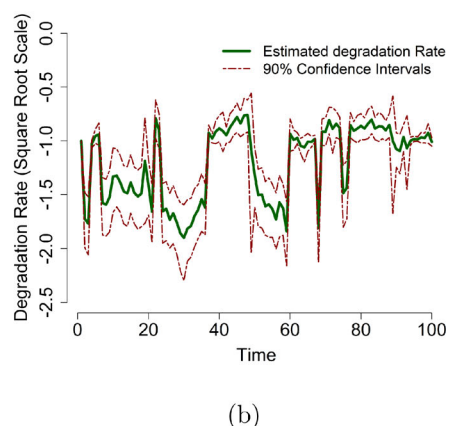


Figure 11. (a) Estimated degradation rate (magnitude in square root) with respect to rotational speed (standardized) and discharge pressure (standardized): the surface in the middle shows the estimated degradation rate, while the surfaces above and below show the 90 percent bootstrap conference intervals, respectively. (b) Estimated degradation rate over time and its 90 percent bootstrap confidence intervals.

rotating motion, abrasion between some friction parts is inevitable (swash plate/slipper, valve plate/cylinder block, and piston/cylinder bore). Continuous abrasion causes the pump to degrade, and the pump degradation is measured as the volume (in milliliter) of return oil per minute. The degradation rate depends on discharge pressure (ranges from 21 to 28 Pa) and rotational speed (ranges from 3,000 to 4,500 rpm).

In our dataset, the degradation data (i.e., the volume of return oil) are aggregated over 10-hour intervals. The degradation level is standardized such that the initial degradation starts from 100. The discharge pressure and rotational speed are also standardized from 0 to 100. The physical relationship between the degradation (i.e., return oil) and operating conditions (i.e., discharge pressure and rotational speed) is known; see Eq. [1]. Hence, the parametric approach is adopted to model the relationship between degradation rate and operating conditions:

$$\mu_t = \frac{dx_t}{dt} = p_t^{\theta_1} \omega_t^{\theta_2} \exp\left(\theta_3 p_t + \theta_4 \omega_t\right)$$
 [37]

where μ_t is the degradation rate at time t, p_t and ω_t are respectively the discharge pressure and rotational speed, and $\{\theta_i\}_{i=1}^4$ are the unknown model parameters to be estimated. Hence, it follows from Eq. [16] that:

$$\kappa_{t} = \frac{\mu_{t}}{\mu_{0}}$$

$$= \exp \{ \log (p_{t}^{\theta_{1}} \omega_{t}^{\theta_{2}}) + (\theta_{3} p_{t} + c_{4} \omega_{t}) - \log (p_{0}^{\theta_{1}} \omega_{0}^{\theta_{2}}) - (\theta_{3} p_{0} + \theta_{4} \omega_{0}) \}.$$
[38]

The degradation model above contains six parameters: μ_0 , σ_0 , and $\{\theta_i\}_{i=1}^4$ $Z\{\theta_i\}_{i=1}^4$. Table 4 shows the

MLE as well as the 90 percent large-sample confidence intervals for the model parameters.

Figure 10 shows the estimated mean degradation path and the 90 percent bootstrap confidence interval. The confidence interval is obtained using the bootstrap method (Efron and Tibshirani 1994; Meeker and Escobar 2014):

- Let θ be a collection of the model parameters, $\theta = (\mu_0, \sigma_0, \theta_1, \theta_2, \theta_3, \theta_4)$. Based on the estimated parameters and covariance matrix, $(\hat{\theta}, \hat{\Sigma})$, a large number of B (B = 2000) bootstrap samples of θ is generated. The generated θ is denoted by $\theta^{(b)}$, b = 1, 2, ..., B.
- A number of B bootstrap degradation paths, $X_t^{(b)}$, are sampled based on $\theta^{(b)}$ for b = 1, 2, ..., B.
- Based on the bootstrap degradation paths, the MLE of the model parameters $\hat{\boldsymbol{\theta}}^{(b)}$, are obtained for $b=1,2,\ldots,B$. Then, based on the estimated model parameters $\hat{\boldsymbol{\theta}}^{(b)}$, a number of B mean degradation paths $\bar{X}_t^{(b)}$ are computed.
- To compute the confidence intervals of the mean degradation path at time t, we sort the bootstrap mean paths $\bar{X}_t^{(b)}$ in increasing order denoted by $\tilde{X}_t^{(b)}$. Then, the approximate 90 percent confidence intervals for the mean degradation path are given by $[\tilde{X}_t^{(l)}, \tilde{X}_t^{(u)}]$ where $l = B \times \Phi_{nor}[2\Phi_{nor}^{-1}(q) + 2\Phi_{nor}^{-1}(\alpha/2)], u = B \times \Phi_{nor} \ [2\Phi_{nor}^{-1}(q) + 2\Phi_{nor}^{-1}(1 \alpha/2)],$ and q is the proportion of $\tilde{X}_t^{(b)}$ that are less than the estimated mean degradation path calculated from $\hat{\theta}$.

Figure 10 shows that the proposed model well explains the degradation data under time-varying operating conditions, and captures the uncertainty associated with the estimated mean degradation path. For example, it is possible to see that the degradation rate (approximately at time 50) suddenly increases due to the change of operating conditions, and this change is accurately captured by the proposed model. The degradation path obtained from the non-parametric approach (h=2 and b=3) is also included in Figure 10. Similar to the observations from Figure 7, the non-parametric approach, without making parametric assumptions on g(z), has comparable performance to the parametric approach. Throughout this paper, the Nelder-Mead algorithm is used to obtain the parametric degradation model (Glaudell, Garcia, and Garcia 1965), while the nonparametric model is obtained by nonlinear optimization algorithms subject to box constraints which force the parameters c_a to be non-negative so that the function g(z) is non-decreasing in z.

To understand how degradation rate changes over time as the operating conditions vary, Figure 11a shows the estimated relationship between the degradation rate and rotational speed and discharge pressure. The 90 percent bootstrap confidence interval is also included in the figure. It is seen that, the harsher the operating conditions (i.e., higher discharge pressure and rotational speed), the higher the degradation rate. Figure 11b shows the evolution of degradation rate over time

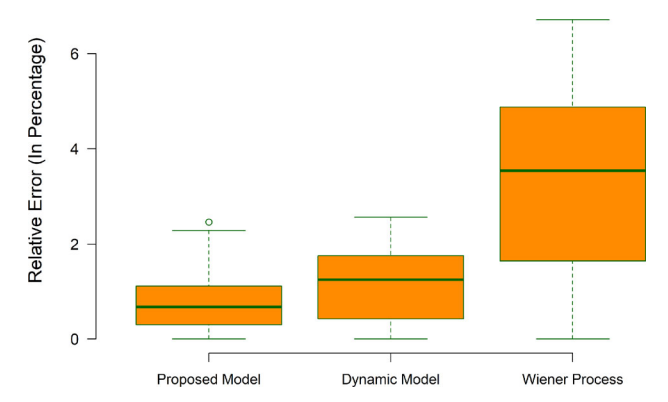


Figure 12. Comparison of the relative error between the proposed model, the dynamical model and the Wiener process model without considering environmental conditions.

as the pressure and rotational speed change. The timedependent variation of degradation rate justifies the importance of modeling the impact of operating conditions on degradation.

Next, we compare the proposed modeling approach to two alternatives: the dynamical model and the Wiener degradation model without considering environmental conditions. The dynamical model used in the comparison study is similar to the one described in Liu, Tan, and Pare (2017) and is given as follows:

$$\Delta Y_t = \mathbf{F}_t \mathbf{\alpha}_t + \varepsilon_t \quad \varepsilon_t \sim \mathcal{N}_r(0, V) \mathbf{\alpha}_t = \mathbf{\alpha}_{t-1} + \mathbf{w}_t \quad \mathbf{w}_t \sim \mathcal{N}_r(0, \mathbf{W})$$
 [39]

where is the increment of degradation level, is the hidden states, ε and \boldsymbol{w} are Gaussian, and $\boldsymbol{F}_t = (p_t, \omega_t)$ contains the operating conditions, where p_t and ω_t are respectively the discharge pressure and rotational speed at time t. The Gibbs sampling algorithm is used to solve at the same time the filtering, smoothing and forecasting problems with unknown parameters.

Figure 12 shows the Boxplot of the relative error for the observed degradation levels between the proposed model, the dynamical model [39] and the Wiener process degradation model without considering environmental conditions. It is seen that the proposed model yields the lowest mean relative error (<1 percent) among all three models. It also clearly shows the importance of taking into account the environmental condition in degradation modeling, as the model without considering such conditions has much worse performance.

3.2. Case study II: Degradation of US highway performance

This section re-visits the second motivating example in Section 1.1, which is concerned with the highway performance degradation in the US and Canada. As discussed in Section 1.1, the highway performance

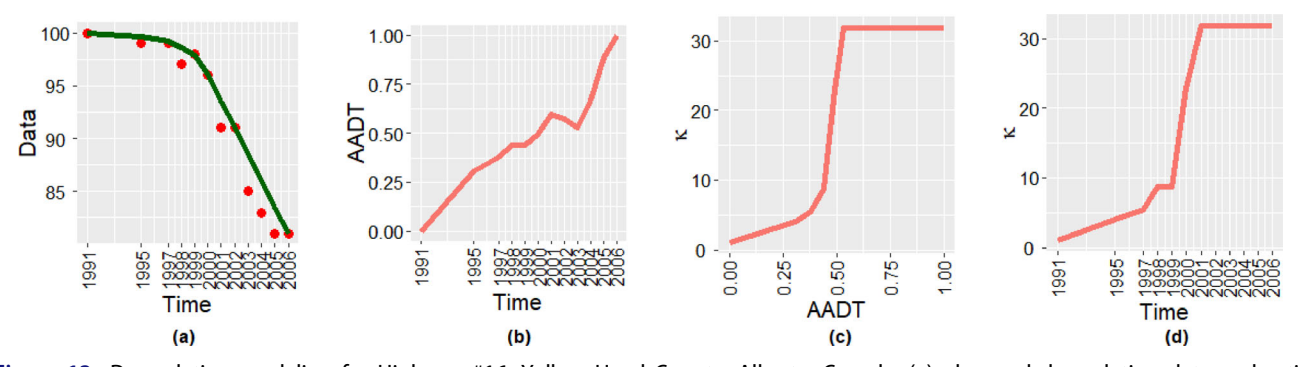


Figure 13. Degradation modeling for Highway #16, Yellow Head County, Alberta, Canada: (a) observed degradation data and estimated mean degradation path; (b) Annual Average Daily Traffic (AADT) over time; (c) estimated $\hat{\kappa}$ which captures the effect of AADT on highway degradation; (d) plot of $\hat{\kappa}$ as AADT changes over time.

(crack length) degrades over time and the degradation rate depends on a number of time-varying environmental factors, especially the traffic volume.

We obtained the data from the Long-Term Pavement Performance (LTPP) Program of the Federal Highway Administration (FHWA) (LTPP 2019). This program collects the pavement performance data from approximately 1,800 highway sections in the US and parts of Canada. It consists of seven modules including inventory, maintenance, monitoring (deflection, distress, and profile), rehabilitation, materials testing, traffic, and climatic. Each road section is associated with a unique SHRP (Strategic Highway Research Program) identification number.

Table 5. Parameter estimation with confidence intervals for case study II.

Parameter	MLE	Asymptotic 90 percent confidence interval
μ	-0.079	(-0.671, 0.513)
σ	0.39	(-1.036, 1.815)
<i>c</i> ₁	1.894	(-6.214, 10.001)
<i>c</i> ₂	1.567	(-0.195, 3.328)
<i>c</i> ₃	0	(-1.622, -8.183)
C ₄	0	(1.622, 2.441)

The processed data have been made available on GitHub (https://github.com/dnncode/LTPP-Data).

For illustrative purposes, we first focus on the data collected from one particular highway section: Highway #16, Yellow Head County, Alberta, Canada. Figure 13a shows the highway performance degradation measured by the crack percentage over time. Here, the degradation level is standardized such that the initial degradation is 100. Figure 13b shows the Annual Average Daily Traffic (AADT) which varies over the years. It is seen from Figure 13a that the road experienced a rapid performance degradation over 1991-2006, over which the AADT significantly increased as clearly shown in Figure 13b. It is interesting to observe that, when AADT slightly dropped over the time period from 2001 to 2003, the road performance degradation appears to be slower over the same time period. After 2003, the AADT started increasing again, causing a rapid road performance degradation. This observation shows the importance to incorporate AADT into the modeling of road performance degradation.

Unlike case study I where the physical relationship between degradation environmental rate and

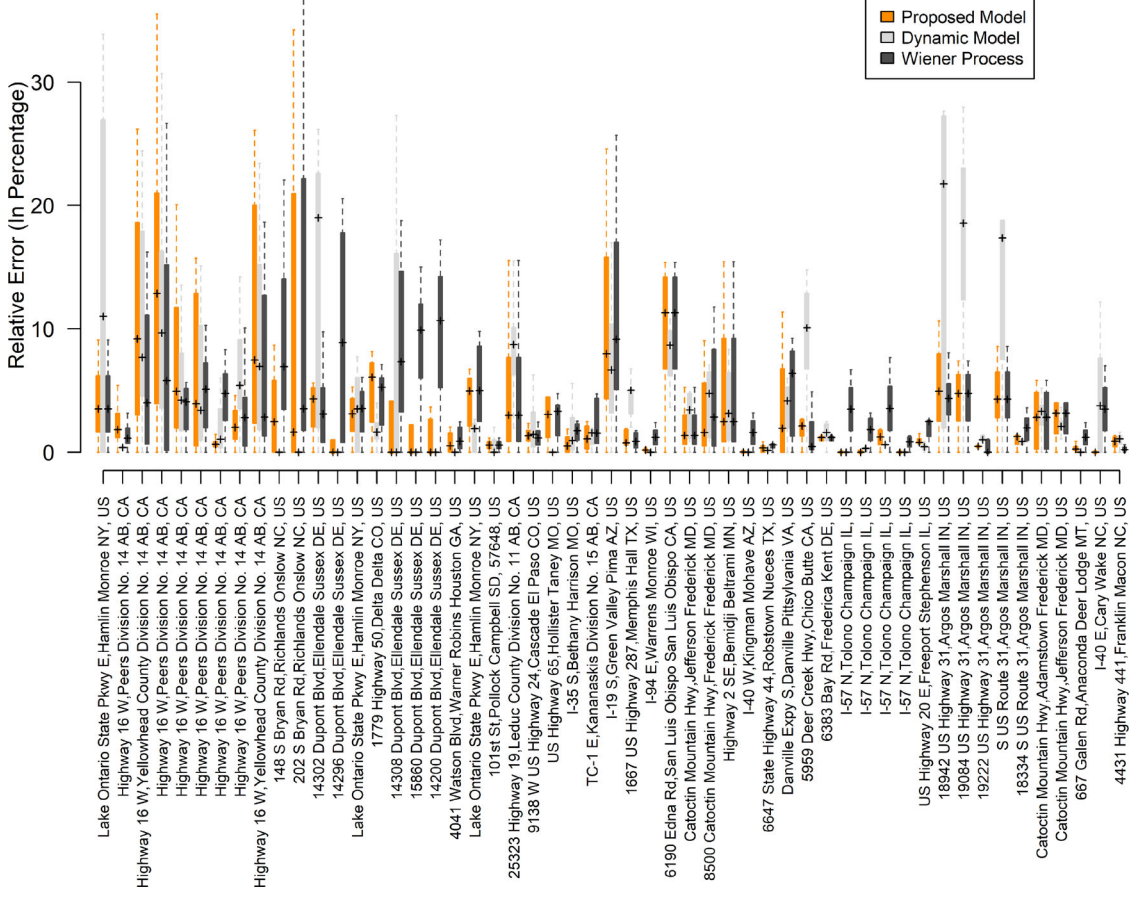


Figure 14. Relative modeling error (in percentage) for the 53 highway sections.

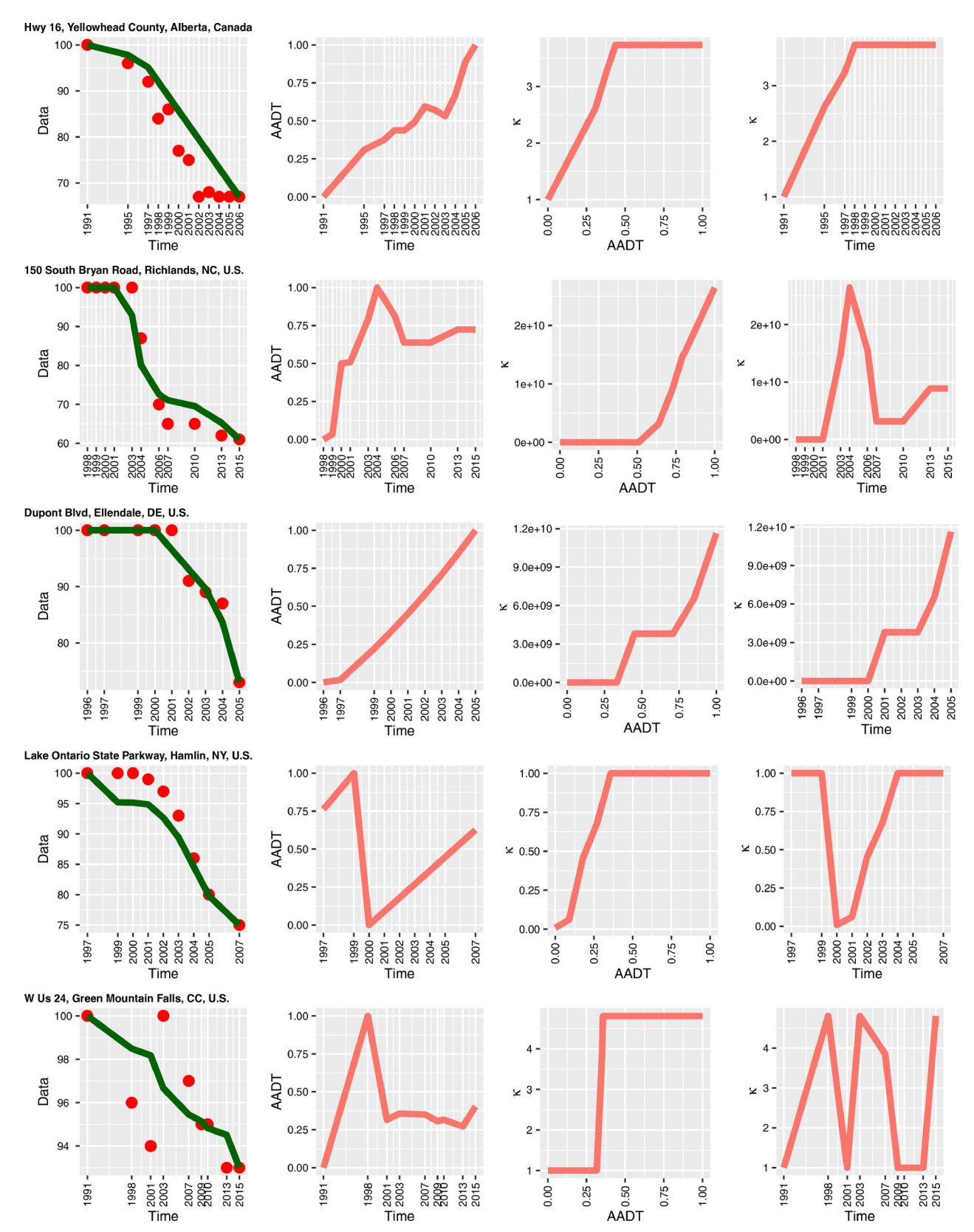


Figure 15. Degradation modeling for U.S. highway performance (road sections 1 to 5).

conditions is known, the complex relationship between highway performance degradation and AADT is not available and is subject to a high level of uncertainty. Hence, in case study II, it is necessary to resort to the non-parametric method, described in Section 2.2.1, in order to capture the effect of traffic

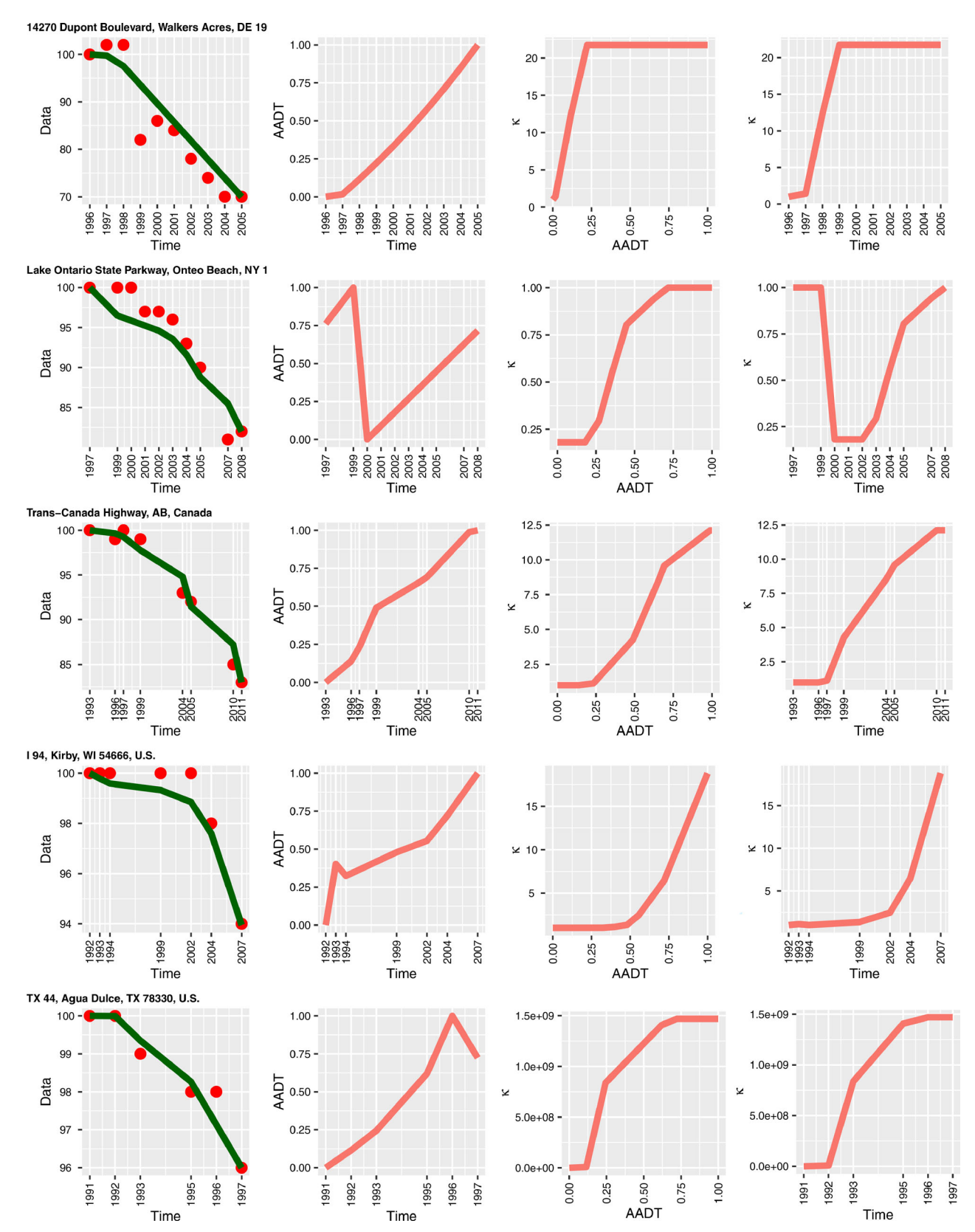


Figure 16. Degradation modeling for U.S. highway performance (road sections 6 to 10).

volume on highway performance degradation. It follows from Eq. [21] that $g(z)=\sum_{q=1}^{q=b+h}c_qI_q^{(h)}(z)$ and $c_q\geq 0$. As discussed in Section 2.2.1, the number of

knots, *b*, depends on the chosen order, *h*, through an empirical relationship, $b \approx n^{\frac{1}{2h+1}}$ as suggested in Ramsay (1998). Table 5 shows the estimated

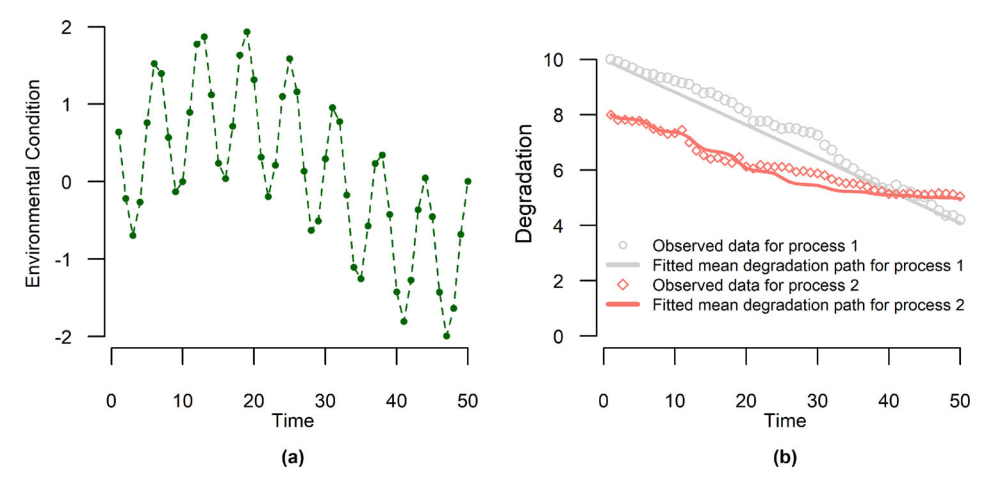


Figure 17. (a) The simulated environmental condition, (b) degradation data for both degradation processes and the estimated mean degradation paths.

parameters as well as the 90 percent large-sample approximate confidence intervals of the model parameters. From Figure 13c, it is observed that κ is non-decreasing function in AADT. Also note that, it appears κ is bounded meaning that the degradation rate does not further increase after the AADT has reached a certain level.

Following the same approach, we model the degradation of a number of 53 highway sections selected from the LTPP dataset. Figure 14 shows the box plot of the relative error (in percentage) for the 53 highway sections. The mean relative error is less than 5 percent for 45 out of the 53 highway sections, while the mean relative error is less than 10 percent for 52 highway sections. Similar to the first case study, Figure 14 also includes the comparison between the proposed model, the dynamical model [39] and the Wiener process degradation without considering the environmental conditions, for the 53 highway sections. The mean (median) relative errors for the three models are respectively, 3.28 percent (2.55 percent), 3.97 percent (3.90 percent), and 4.02 percent (3.55 percent), demonstrating the performance of the proposed model.

To further illustrate the modeling performance, the constructed degradation models are shown for 10 selected road sections; see Figures 15 and 16. It is seen that, the proposed approach well models the degradation of highway performance, as well as the complicated interactions between degradation rate and traffic volume.

3.3. Reliability prediction under competing degradation processes

In the third numerical example, we investigate the reliability prediction for a system subject to two competing degradation processes and dynamic environmental conditions. Of interest is the system reliability over some future time intervals, given the degradation data observed up to time τ ; as described in Section 2.1.

Degradation data are simulated over the time interval [0, 50]. In particular, the first degradation process does not depend on environmental condition by letting $\kappa_t = 1$, while the second degradation process is influenced by the environmental condition through a function $\kappa_t = \exp(\theta^{-1}(z_t - z_0))$. The environmental condition and simulated degradation data over [0, 50] are shown in Figure 17. The model involves five parameters, $(\mu_0^{(1)}, \mu_0^{(2)}, \sigma_0^{(1)}, \sigma_0^{(2)}, \theta)$, which can be found by maximizing the log-likelihood function (Eq. [31]). In this example, the ML estimates are $\hat{\mu}_0^{(1)} = -0.16$, $\hat{\mu}_0^{(2)} = -0.12$, $\hat{\sigma}_0^{(1)} = 0.12$, $\hat{\sigma}_0^{(2)} = 0.08$ and $\hat{\theta} = 0.12$ 0.89. The estimated mean paths of the two degradation processes are shown in Figure 17b by solid lines. Conditioning on the observed degradation data up to time $\tau = 50$, the system reliability depends on the future environmental condition z_t for $t > \tau$. However, the environmental condition from the last observation time τ onward can rarely be known exactly, and the predicted environmental condition is always subject to prediction error. For example, although one might be able to predict the temperature fluctuation or trend, the actual temperature is likely to vary around the predicted values. In this numerical example, we denote the environmental condition over a future time interval $[\tau, \tau + \Delta]$ by $Z_{\nu} = \alpha_{\nu} + \varepsilon_{\nu}$, where $\nu =$ $t-\tau, \alpha_{\nu}$ is a deterministic function, and ε_{ν} is a zeromean stochastic process, i.e., $\mathbb{E}(\varepsilon_{\nu}) = 0$. The choice of ε_{ν} is case-dependent. For example, ε_{ν} can be simply chosen as a normal white noise or a random processes which captures the temporal correlation of the environmental condition. For illustrative purposes, we let ε_{ν} be a Brownian motion in this example with mean zero and time-dependent variance $\sigma_{\varepsilon}^2 \nu$, reflecting the

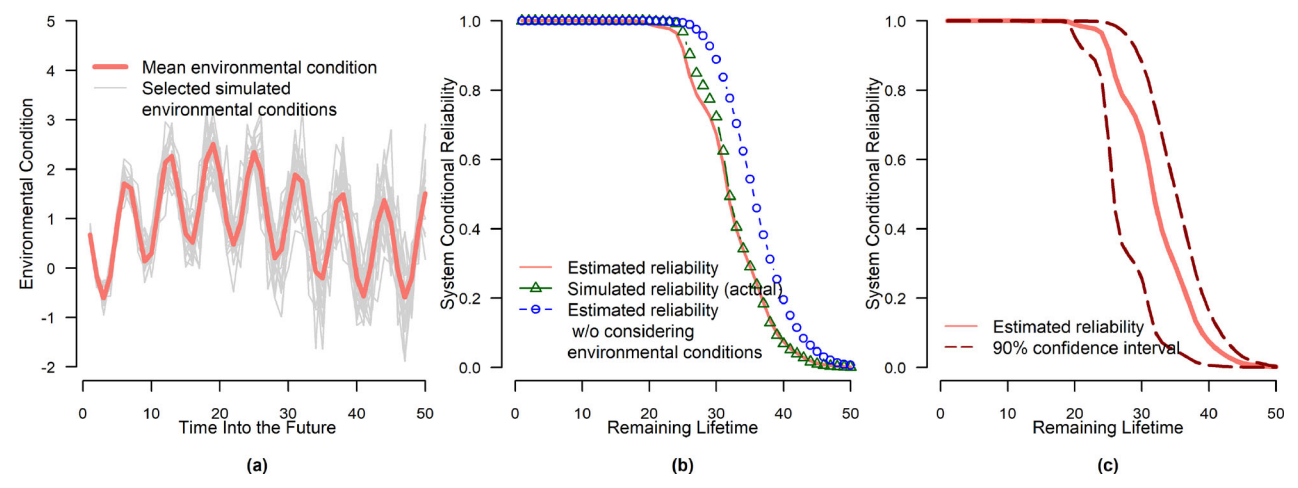


Figure 18. (a) 20 randomly selected simulated environmental conditions as well as the mean environmental condition computed from the 5,000 simulated samples; (b) Estimated reliability functions and the actual reliability obtained from simulation; (c) Estimated reliability function with 90 percent bootstrap confidence interval.

fact that the environmental condition becomes more difficult to be predicted as ν increases.

Conditioning on the last observed degradation at time τ , the system reliability under changing environmental condition Z_{ν} is given by

$$R(\nu) = \mathbb{E}_{Z_{\nu}} \{ G(\nu^{(1)}, \nu^{(2)})_{\nu:1_{2}} \}$$
 [40]

where $G(\nu^{(1)}, \nu^{(2)})$ can be found in Section 2.1. The computation of Eq. [40] is complex since the expectation is taken with respect to the σ -algebra, $\sigma\{z_{\nu}, 0 \leq \nu \leq \Delta\}$, generated by the entire future paths of the environmental condition. A simulation-based procedure is thus adopted to compute the system reliability as follows:

Step 1: Generate a large number of realizations of the environmental condition from the stochastic process $Z_{\nu} = \alpha_{\nu} + \sigma_{\nu}$ for $0 \le \nu \le \Delta$, and denote the m^{th} simulated environmental condition by $Z_{\nu}^{(m)}$ for m = 1, 2, ...M.

Step 2: For each realization of the environmental condition, compute the probabilities that the system fails due to one of the two degradation processes from Proposition 1:

$$P_{\Delta}^{(1)} = \int_{0}^{\Delta} \xi_{1}(\nu^{(2)}) \xi_{2}(\nu^{(1)})_{\nu \cdot 1_{2}} d\nu$$
 [41]

$$P_{\Delta}^{(2)} = \int_{0}^{\Delta} \xi_{1}(\nu^{(1)}) \xi_{2}(\nu^{(2)})_{\nu \cdot 1_{2}} d\nu$$
 [42]

and compute the system reliability for given as follows:

$$R^{(m)}(\nu) = G(\nu^{(1)}, \nu^{(2)}), \quad 0 \le \nu \le \Delta.$$
 [43]

Step 3: Calculate the system reliability, $R(\nu)$, under stochastic environment by averaging $R^{(m)}(\nu)$:

$$R(\nu) \approx \hat{R}(\nu) = \frac{1}{M} \sum_{m=1}^{M} R^{(m)}(\nu)$$
 [44]

In other words, the system reliability is approximated by the sample mean. Since M is finite in practice, for any $0 \le \nu \le \Delta$, it follows from the Central Limit Theorem that $\hat{R}(\nu) \overset{\mathrm{d}}{\to} N(0, \sigma_M^2)$ where the variance can be estimated by $\hat{\sigma}_M^2 = M^{-1} \sum_{m=1}^M (R^{(m)}(\nu) - R(\nu))^2$ Hence, the approximation (Eq. [44]) can be made sufficiently accurate due to the law of large numbers, i.e., $\hat{R}(\nu) \to R(\nu)$ as $M \to \infty$.

In this numerical example, suppose that the future environmental condition is stochastic and can be represented by:

$$Z_{\nu} = 0.03\nu + \sin(0.1\nu) + \cos(\nu) + \varepsilon_{\nu}, \quad 0 \le \nu \le \Delta$$
[45]

where $\Delta = 50$, and ε_{ν} is a Brownian motion with mean zero with time-dependent variance $\sigma_{\varepsilon}^2 \nu$ and $\sigma_{\varepsilon} = 0.1$. Hence, the future environment is stochastic and the uncertainty grows in time. Following the procedure described above, we obtain, from a large number of iterations N = 5,000, the system reliability, $R(\nu)$, over the time interval [0, 50]. Figure 18a shows 20 randomly selected simulated environmental conditions as well as the average environmental condition computed from the 5,000 simulated samples. Figure 18b shows the comparison between the estimated reliability and actual reliability function obtained from simulation. In particular, we simulate the future degradation paths and obtain the actual failure times. Then, the Kaplan-Meier (KM) method is used to obtain the empirical (conditional) reliability. It is seen that, the estimated reliability function well matches with the empirical reliability obtained from simulated

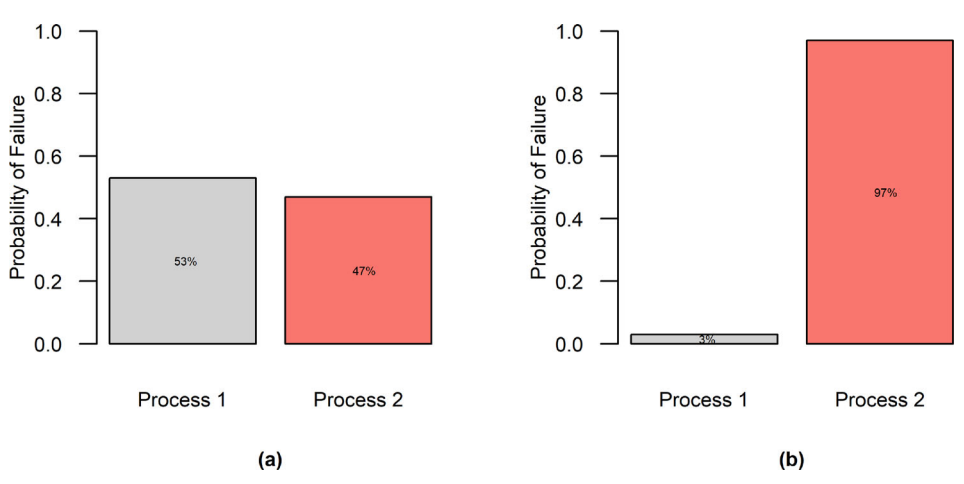


Figure 19. Probabilities that the system fails due to one of the two competing degradation processes: (a) the environmental condition is based on Eq. [45]; (b) the environmental condition is based on Eq. [46].

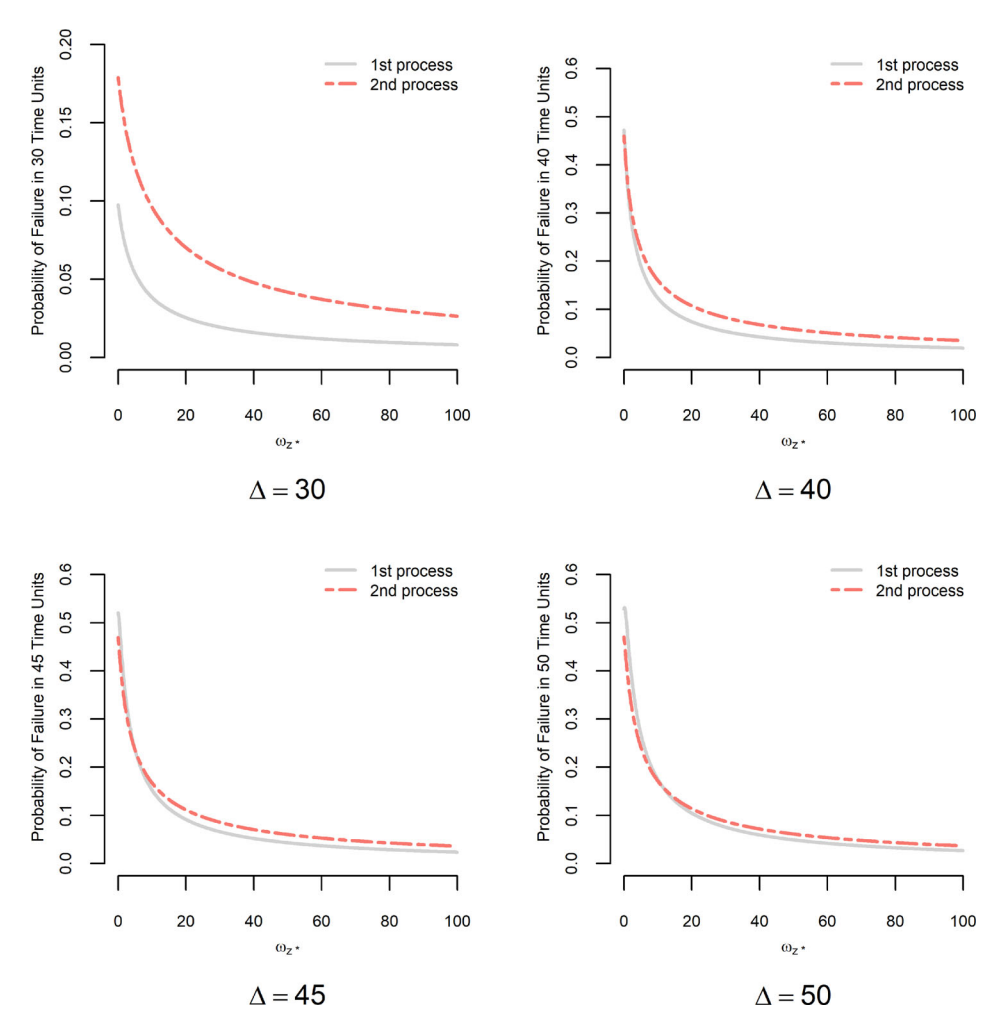


Figure 20. Probabilities that the system fails due to one of the two competing processes for ω_{Z*} ranges from 0 to 100 and for $\Delta = 30, 40, 45, 50$.

failure data. In Figure 18b, we also include the estimated conditional reliability ignoring the environmental conditions, which clearly over-estimates the system reliability. Figure 18c shows the estimated reliability

with its 90 percent confidence interval obtained from the bootstrap samples $R^{(m)}(\nu)$ in Eq. [43].

Using the results presented in Proposition 1, Figure 19a shows the probabilities that the system fails over a

future time interval (50, 100) due to degradation processes 1 or 2 are respectively 0.53 and 0.47 (note that, $\tau = 50$ which is the current time and $\Delta = 50$). Since the sum of $P_{50}^{(1)}$ and $P_{50}^{(2)}$ is approximately one, the system will almost certainly fail within the next 50 time periods. For comparison purposes, we modify the linear component in Eq. [45], and let the new changing environmental condition be denoted by

$$Z_{\nu} = 0.05\nu + \sin(0.1\nu) + \cos(\nu) + \varepsilon_{\nu}, \quad 0 \le \nu \le \Delta.$$
 [46]

Figure 19b shows the new probabilities that the system fails due to one of the two competing degradation processes. See that, since the modified environmental condition (Eq. [46]) is severer than that defined in Eq. [45], degradation process 2 (which is influenced by the environment condition) naturally becomes the dominant cause of failure: the probability that the system fails due to degradation process 2 increases to 97 percent from 47 percent. This significant change strongly demonstrates the importance of taking into account environmental and operating conditions for reliability prediction using degradation data.

As discussed in Section 2.1, it is common that the multiple degradation processes are influenced by some common but unknown random environmental factor Z^* . As a result, the latent remaining lifetime of the two competing degradation processes become dependent, which is modeled by a Gamma Frailty model; see Proposition 2. Assuming that the Gamma frailty has mean one and variance ω_{Z*} , Figure 20 shows the probabilities that the system fails due to one of the two competing processes for ω_{Z*} ranges from 0 to 100, and for $\Delta = 30, 40, 45, 50$. The environmental condition still follows [45].

Figure 20a shows that the system is more likely to fail due to the first degradation process in the next 30 time periods. However, in the next 40, 45, and 50 time periods, the probabilities that the system fails due to the second degradation process becomes higher as shown in Figure 20b,c. This is precisely due to the fact that the future environmental condition [45] is getting severer, causing a higher degradation rate of the second process. Note that, only the second degradation process is influenced by the environmental condition in this example. As ω_{Z*} becomes larger (i.e., the statistical dependence between the latent remaining lifetimes become stronger), the probabilities that the system respectively fails due to processes 1 and 2 become lower simultaneously, indicating higher system reliability. This can be seen from Eq. [13] where the joint survival function is monotone increasing in

 ω_{Z*} . Hence, it is clearly demonstrated that the predicted reliability can be very different with and without considering the environmental conditions. Such observations strongly justify the importance of including environmental and operating conditions into reliability analysis using degradation data.

4. Conclusion

This paper investigated the degradation modeling under dynamic environmental conditions. The main results can be applied to both univariate degradation and a more general case with multiple competing degradation processes. Parametric and non-parametric approaches have been employed to capture the effect of dynamic environmental conditions on degradation. The Wiener process was used to describe individual degradation processes, and the remaining lifetime distribution has been obtained for individual processes. Leveraging the classical competing risks model, this paper obtained the probability that the system fails due to a particular degradation process over a given future time interval of interest, provided with the degradation data observed up to a certain point in the past. A Gamma frailty model has been adopted to capture the statistical dependency among latent remaining lifetimes of multiple degradation processes, due to some common but unobserved external factors. Such a result can serve an extremely important role in practice for system health prognostics and predictive maintenance planning. The applications of the proposed approach have been illustrated through two case studies and comprehensive numerical studies based on simulated data. These numerical experiments not only demonstrated the effectiveness of the proposed approach, but also strongly justified the importance and necessity of taking into account dynamic environmental and operating conditions in reliability analysis based on degradation data. The model is motivated by the well-known Nelson's Cumulative Exposure (CE) model, implying that the ratio between the drift and diffusion coefficients remains unchanged. Like any modeling assumptions, the assumption adds additional constraints to the model. Fortunately, even if such an equation does not hold, the proposed modeling framework still works but the first passage time distribution can only be obtained through simulation or approximation. In other words, the closed-form expression of the remaining life distribution is no longer available, but can be approximated numerically through simulation.



About the authors

Mohammadmahdi Hajiha is a Ph.D. candidate at the Department of Industrial Engineering, University of Arkansas. His e-mail address is mhajiha@uark.edu

Xiao Liu is an Assistant Professor at the Department of Industrial Engineering, University of Arkansas. His email address is liuxiao314923@gmail.com

Yili Hong is an Associate Professor at the Department of Statistics, Virginia Tech. His e-mail address is yilihong@vt.edu

Funding

National Science Foundation, #1904165.

References

- Abbring, J. H., and G. J. Van Den Berg. 2007. The unobserved heterogeneity distribution in duration analysis. Biometrika 94 (1):87-99. doi: 10.1093/biomet/asm013.
- Bhattacharyya, G., and A. Fries. 1982. Fatigue failure models-Birnbaum-Saunders vs. inverse Gaussian. IEEE Transactions on Reliability R-31 (5):439-41. doi: 10.1109/ TR.1982.5221421.
- Bian, L., and N. Gebraeel. 2012. Computing and updating the first-passage time distribution for randomly evolving degradation signals. IIE Transactions 44 (11):974-87. doi: 10.1080/0740817X.2011.649661.
- Bian, L., and N. Gebraeel. 2013. Stochastic methodology for prognostics under continuously varying environmental profiles. Statistical Analysis and Data Mining 6 (3): 260-70.
- Bian, L., N. Gebraeel, and J. Kharoufeh. 2015. Degradation modeling for real-time estimation of residual lifetimes in dynamic environments. IIE Transactions 47 (5):471-86. doi: 10.1080/0740817X.2014.955153.
- Birnbaum, Z. W., and S. C. Saunders. 1969. A new family of life distributions. Journal of Applied Probability 6 (2): 319-27. doi: 10.2307/3212003.
- Chehade, A., C. Song, K. Liu, A. Saxena, and X. Zhang. 2018. A data-level fusion approach for degradation modeling and prognostic analysis under multiple failure modes. Journal of Quality Technology 50 (2):150-65. doi: 10.1080/00224065.2018.1436829.
- Chen, P., and Z.-S. Ye. 2018. Uncertainty quantification for monotone stochastic degradation models. Journal of Quality Technology 50 (2):207-19. doi: 10.1080/00224065. 2018.1436839.
- Cox, D., and H. Miller. 1965. The theory of stochastic processes. Boca Raton: CRC Press.
- Crowder, M. J. 2001. Classical competing risks. Boca Raton: Chapman and Hall/CRC.
- Doksum, K. A., A. Hóyland, and A. Hoyland. 1992. Models for variable-stress accelerated life testing experiments based on Wiener processes and the inverse Gaussian distribution. Technometrics 34 (1):74-82. doi: 10.2307/ 1269554.
- Efron, B., and R. J. Tibshirani. 1994. An introduction to the bootstrap. Boca Raton: Chapman and Hall/CRC.

- Elsayed, E. A. 2012. Reliability engineering, vol. 88. Hoboken: John Wiley & Sons.
- Elwany, A., and N. Gebraeel. 2009. Real-time estimation of mean remaining life using sensor-based degradation models. Journal of Manufacturing Science and Engineering 131 (5):051005-9. doi: 10.1115/1.3159045.
- Fang, G., R. Pan, and Y. Hong. 2020. Copula-based reliability analysis of degrading systems with dependent failures. Reliability Engineering and System Safety 193:106618.
- Fang, X., K. Paynabar, and N. Gebraeel. 2019. Image-based prognostics using penalized tensor regression. Technometrics 61 (3):369-384. doi: 10.1080/00401706. 2018.1527727.
- Gebraeel, N., and J. Pan. 2008. Prognostic degradation models for computing and updating residual life distributions in a time-varying environment. IEEE Transactions on Reliability 57:539-550. doi: 10.1109/TR.2008.928245.
- Glaudell, R., R. T. Garcia, and J. B. Garcia. 1965. Neldermead simplex method. The Computer Journal 7 (4): 308-313. doi: 10.1093/comjnl/7.4.308.
- Hong, L., M. H. Y. Tan, and Z.-S. Ye. 2019. Nonparametric link functions with shape constraints in stochastic degradation processes: Application to emerging contaminants. Journal of Quality Technology, 1-15. doi: 10.1080/ 00224065.2019.1611353.
- Hong, Y., Y. Duan, W. Q. Meeker, D. L. Stanley, and X. Gu. 2015. Statistical methods for degradation data with dynamic covariates information and an application to outdoor weathering data. Technometrics 57 (2):180-193. doi: 10.1080/00401706.2014.915891.
- Hong, Y., M. Zhang, and W. Q. Meeker. 2018. Big data and reliability applications: The complexity dimension. Journal of Quality Technology 50 (2):135-149. doi: 10. 1080/00224065.2018.1438007.
- Huang, T., B. Peng, D. W. Coit, and Z. Yu. 2019. Degradation modeling and lifetime prediction considering effective shocks in a dynamic environment. IEEE Transactions on Reliability 68 (3):819-830. doi: 10.1109/ TR.2019.2917058.
- Jiang, L., Q. Feng, and D. W. Coit. 2015. Modeling zoned shock effects on stochastic degradation in dependent failure processes. IIE Transactions 47 (5):460-470. doi: 10. 1080/0740817X.2014.955152.
- Jin, R., X. Deng, X. Chen, L. Zhu, and J. Zhang. 2019. Dynamic quality-process model in consideration of equipment degradation. Journal of Quality Technology 51 (3):217-13. doi: 10.1080/00224065.2018.1541379.
- Kharoufeh, J. P. 2003. Explicit results for wear processes in a Markovian environment. Operations Research Letters 31 (3):237-244. doi: 10.1016/S0167-6377(02)00229-8.
- Liao, H., and E. A. Elsayed. 2006. Reliability inference for field conditions from accelerated degradation testing. Naval Research Logistics 53 (6):576-587. doi: 10.1002/nav.20163.
- Liao, H., and Z. Tian. 2013. A framework for predicting the remaining useful life of a single unit under time-varying operating conditions. IIE Transactions 45 (9):964-980. doi: 10.1080/0740817X.2012.705451.
- Liu, B., X. Zhao, G. Liu, and Y. Liu. 2020. Life cycle cost analysis considering multiple dependent degradation processes and environmental influence. Reliability Engineering and System Safety 197:106784.



- Liu, K., A. Chehade, and C. Song. 2017. Optimize the signal quality of the composite health index via data fusion for degradation modeling and prognostic analysis. IEEE Transactions on Automation Science and Engineering 14 (3):1504–1542. doi: 10.1109/TASE.2015.2446752.
- Liu, X. 2012. Planning of accelerated life tests with dependent failure modes based on a gamma frailty model. Technometrics 54 (4):398-409. doi: 10.1080/00401706. 2012.707579.
- Liu, X., J. Li, K. N. Al-Khalifa, A. S. Hamouda, D. W. Coit, and E. A. Elsayed. 2013. Condition-based maintenance for continuously monitored degrading systems with multiple failure modes. IIE Transactions 45 (4):422-435. doi: 10.1080/0740817X.2012.690930.
- Liu, X., and W. S. Qiu. 2011. Modeling and planning of step-stress accelerated life tests with independent competing risks. IEEE Transactions on Reliability 60 (4):712–720. doi: 10.1109/TR.2011.2160748.
- Liu, X., C. T. Tan, and D. Pare. 2017. A case study on the modeling of system state degradation for data center cooling systems. In Proceedings of the 2017 Prognostics and System Health Management Conference, IEEE, Harbin, China.
- Liu, X., K. M. Yeo, and J. Kalagnanam. 2018. A statistical modeling approach for spatio-temporal degradation data. Journal of Quality Technology 50 (2):166-182. doi: 10. 1080/00224065.2018.1436833.
- LTPP. 2019. Long-term pavement performance. Department of Transportation, Federal Highway Administration. https://highways.dot.gov/research/long-term-infrastructureperformance/ltpp/long-term-pavement-performance
- Ma, Z. H., S. P. Wang, H. T. Liao, and C. Zhang. 2019. Engineering-driven performance degradation analysis of hydraulic piston pump based on the inverse Gaussian process. Quality and Reliability Engineering International 35:2278-2296. doi: 10.1002/gre.2502.
- Meeker, W. Q., and L. A. Escobar. 2014. Statistical methods for reliability data. New York: John Wiley & Sons.
- Meeker, W. Q., and Y. Hong. 2014. Reliability meets Big Data: Opportunities and challenges. Quality Engineering 26 (1):102-116. doi: 10.1080/08982112.2014.846119.
- Meyer, M. C. 2008. Inference using shape-restricted regression splines. The Annals of Applied Statistics 2 (3): 1013-1033. doi: 10.1214/08-AOAS167.
- Nelson, W. B. 2009. Accelerated testing: Statistical models, test plans, and data analysis, vol. 344. Hoboken: John Wiley & Sons.
- Peng, C.-Y., and S.-T. Tseng. 2010. Progressive-stress accelerated degradation test for highly-reliable products. IEEE *Transactions on Reliability* 59:30–7.
- Peng, W., Y.-F. Li, J. Mi, L. Yu, and H.-Z. Huang. 2016. Reliability of complex systems under dynamic conditions: Bayesian multivariate degradation perspective. Reliability Engineering & System Safety 153:75-87. doi: 10.1016/j.ress.2016.04.005.

- Rafiee, K., Q. Feng, and D. W. Coit. 2014. Reliability modeling for dependent competing failure processes with changing degradation rate. IIE Transactions 46 (5): 483-496. doi: 10.1080/0740817X.2013.812270.
- Ramsay, J. O. 1998. Estimating smooth monotone functions. Journal of the Royal Statistical Society: Series B (Statistical Methodology) 60 (2):365-375. doi: 10.1111/1467-9868. 00130.
- Shen, J., and L. Cui. 2016. Reliability performance for dynamic systems with cycles of K regimes. IIE Transactions 48 (4):389-402. doi: 10.1080/0740817X.2015. 1110266.
- Singpurwalla, N. D. 1995. Survival in dynamic environments. Statistical Science 10 (1):86-103. doi: 10.1214/ss/ 1177010132.
- Song, C., K. Liu, and X. Zhang. 2018. Integration of datalevel fusion model and kernel methods for degradation modeling and prognostic analysis. IEEE Transactions on Reliability 67 (2):640-650. doi: 10.1109/TR.2017.2715180.
- Thomas, E. V., I. Bloom, J. P. Christophersen, D. C. Robertson, L. K. Walker, C. D. Ho, and V. S. Battaglia. 2019. Modeling memoryless degradation under variable stress. Journal of Quality Technology 51 (3):284-16. doi: 10.1080/00224065.2019.1569963.
- Tian, Z., and H. Liao. 2011. Condition based maintenance optimization for multi-component systems using proportional hazards model. Reliability Engineering & System Safety 96 (5):581-589. doi: 10.1016/j.ress.2010.12.023.
- Tseng, S.-T., and C.-Y. Peng. 2004. Optimal burn-in policy by using an integrated Wiener process. IIE Transactions 36 (12):1161-1170. doi: 10.1080/07408170490507701.
- Yan, H., K. Liu, X. Zhang, and J. Shi. 2016. Multiple sensor data fusion for degradation modeling and prognostics under multiple operational conditions. IEEE Transactions on Reliability 65 (3):1416-1426. doi: 10.1109/TR.2016. 2575449.
- Yang, L., Y. Zhao, R. Peng, and X. Ma. 2018. Hybrid preventive maintenance of competing failures under random environment. Reliability Engineering & System Safety 174: 130-140. doi: 10.1016/j.ress.2018.02.017.
- Ye, Z.-S., and N. Chen. 2014. The inverse Gaussian process as a degradation model. Technometrics 56 (3):302-311. doi: 10.1080/00401706.2013.830074.
- Zhai, Q., and Z.-S. Ye. 2018. Degradation in common dynamic environments. Technometrics 60 (4):461-471. doi: 10.1080/00401706.2017.1375994.
- Zhao, X. J., J. Xu, and B. Liu. 2018. Accelerated degradation tests planning with competing failure modes. IEEE Transactions on Reliability 67 (1):142-155. doi: 10.1109/ TR.2017.2761025.
- Zhou, R., N. Serban, and N. Gebraeel. 2014. Degradationbased residual life prediction under different environments. The Annals of Applied Statistics 8 (3):1671-1689. doi: 10.1214/14-AOAS749.